M 2015

U.PORTO
FEUP FACULDADE DE ENGENHARIA
UNIVERSIDADE DO PORTO

MODELLING AND VALIDATION OF CO_2 CAPTURE PROCESSES WITH PIPERAZINE

MARIANA RODRIGUES FERREIRA DE SOUSA GOMES

DISSERTAÇÃO DE MESTRADO APRESENTADA
À FACULDADE DE ENGENHARIA DA UNIVERSIDADE DO PORTO EM
ENGENHARIA QUÍMICA

Integrated Master in Chemical Engineering

Modelling and validation of CO_2 Capture Processes with Piperazine

Master Thesis

of

Mariana Rodrigues Ferreira de Sousa Gomes

Developed in the context of the Dissertation course

carried out in

Process Systems Enterprise Ltd.

Supervisors at FEUP:

Dr. Ana Mafalda Ribeiro, Dr. José Miguel Loureiro

Supervisor at PSE:

Dr. Javier Rodriguez

Department of Chemical Engineering

July 2015

Acknowledgments

First of all, I would like to express my appreciation to Prof. Dr. Luís Miguel Madeira and especially to Prof. Dr. Costas Pantelides for providing me the amazing opportunity of taking an internship at Process Systems Enterprise Limited and for all the financial support.

To my supervisors Dr. Javier Rodriguez, Dr. Ana Mafalda Ribeiro and Prof. Dr. José Miguel Loureiro, for all the interest demonstrated in my work and for the availability every time I needed help.

I would also like to thank everyone at PSE, particularly the Power & CCS team, with whom I had the pleasure of working during these five months.

To my fellow interns Byeonggil, Gabriele, Giovanni, Joana, João, Miguel, Sancho and Yera, with whom I got to share my best and worst times. A special acknowledgment to JJ, that besides all the fun moments contributed a lot to the development of my thesis, providing me bright ideas at the right time. And to Fred, my gym partner, who actually made me enjoy waking up two hours earlier to work out.

To Ana and Helena, my neighbours and friends, the ones who started, lived and finished this journey with me. Thank you for your kind and positive words in the hardest times.

Last but not least, I would like to show my deepest gratitude to my family and friends, especially my parents, my sisters, Beatriz and Carolina, and Gil, for all the care and support in every moment of my life. Even thousands of miles away, they never let me feel alone.

This page was intentionally left blank.

Abstract

The present thesis describes the work developed within the Dissertation course throughout an academic internship at Process Systems Enterprise Limited, in the context of chemical absorption processes for carbon dioxide (CO_2) capture. Almost half of the worldwide CO_2 emissions are due to the combustion of fossil fuels for energy production, which shows that its capture and sequestration from power plants would represent a significant reduction in carbon emissions.

The main objective of the present thesis is to model and compare the performance of different process configuration solutions for the removal of CO_2 from flue gases employing piperazine as solvent. Flowsheet models were assembled for five configurations using gPROMS® ModelBuilder 4.1.0. The base case used for comparison is the conventional process for amine scrubbing, whose main components are a simple absorber and a simple stripper. New equipment units were incorporated in the simple flowsheet, successfully improving the energy requirements. In order to ensure an objective and consistent analysis of the solvent and each configuration studied, the models were validated with experimental data publically available provided by "The Rochelle Lab", placed at the University of Texas at Austin. CO_2 capture rate presented a maximum deviation of $-12\ \%$, and the rich loading shown even lower deviations: between -3 and $5\ \%$.

Besides comparing heat duty and CO_2 capture for all the configurations, a sensitivity analysis was made to understand the effect of intercooling temperature, intercooling position, stripping pressure, L/G ratio and piperazine concentration on the results.

Three of the analysed processes were optimised in order to minimize the energy requirements, and a maximum decrease of $19\ \%$ was achieved.

Key-words: carbon capture and storage, post-combustion capture, chemical absorption, piperazine, gPROMS®.

This page was intentionally left blank.

Resumo

O presente documento descreve o trabalho desenvolvido no âmbito da unidade curricular de Dissertacão ao longo de um estágio académico realizado na empresa *Process Systems Enterprise*, no contexto de processos de absorção química para captura de carbono. Quase metade das emissões globais de dióxido de carbono são originadas pela combustão de combustíveis fósseis para produção energética, pelo que a sua captura em centrais elétricas representaria uma redução significativa nas emissões de carbono.

O objectivo principal desta tese é simular e comparar o desempenho de diferentes configurações para a remoção de CO_2 a partir de gases de combustão, usando a piperazina como solvente. No gPROMS® ModelBuilder 4.1.0 foram construídos os *flowsheets* correspondentes a cinco configurações diferentes. O modelo usado para comparação corresponde ao processo convencional de captura de carbono com aminas, cujos componentes principais são colunas de absorção e dessorção simples. No caso mais simples foram incorporados novos equipamentos, cumprindo o objectivo de melhorar as necessidades energéticas. De forma a garantir uma análise objectiva e consistente do solvente e de cada configuração estudada, os modelos foram validados através da sua comparação com dados experimentais disponíveis publicamente, provenientes do "The Rochelle Lab", um laboratório pertencente à Universidade do Texas em Austin. A captura de CO_2 apresentou um desvio máximo de -12 % e o *rich loading* apresentou desvios ainda menores: entre -3 and 5 %.

Além de comparar o calor necessário para a captura de CO_2 em cada configuração, análises de sensibilidade foram efectuadas para compreender os efeitos do arrefecimento intermédio e da posição do mesmo na coluna de absorção, da pressão da etapa de dessorção, da razão entre os caudais de líquido e vapor e da concentração do solvente nos resultados finais.

Três das configurações analisadas foram optimizadas de modo a minimizar as necessidades energéticas, e um diminuição máxima de 19 % foi conseguida.

Palavras-chave: captura e armazenamento de carbono, captura de pos-combustão, absorção química, piperazina, gPROMS®.

This page was intentionally left blank.

Declaração

Declara, sob compromisso de honra, que este trabalho é original e que todas as contribuições não originais foram devidamente referenciadas com identificação da fonte.

Mariana Rodrigues Ferreira de Sousa Gomes

06/07/2015

This page was intentionally left blank.

Contents

List of figures

List of Tables

List of Abbreviations

A	Chemical absorber
aMDEA	Activated methyldiethanolamine
C	Condenser
CCS	Carbon Capture and Storage
DEA	Diethanolamine
DIPA	Diisopropanolamine
EOR	Enhanced oil recovery
F	Flash drum
FG	Flue gas
HX	Integrated heat exchanger
HXU	Heat exchanger using an utility
IC	Intercooling
IGCC	Integrated Gasification Combined Cycle
LS	Lean solvent
M	Junction
MDEA	Methyldiethanolamine
MEA	Monoethanolamine
MSEP	Mean squared error of prediction
P	Pump simple
PCC	Post-Combustion Capture
PSE	Process Systems Enterprise limited
PZ	Piperazine
R	Reboiler
RB	Recycle breaker
RS	Rich solvent
S	Process sink
SAFT	Statistical associating of fluid theory
SMU	Solvent make-up
SR	Process source
SRU	Utility source
ST	Chemical stripper
SU	Utility sink
TG	Treated gas

List of symbols

Variable	Description	Unit
C_P	Specific heat	kJ/(kg·K)
F	Mass flow rate	kg/s
H	Heat duty	kJ/s
N_{Runs}	Number of experimental runs	-
P	Pressure	bar, atm or Pa
T	Temperature	K or °C
w	Mass fraction	g/g
x	Molar fraction	mol/mol
Z	Column position	m
Z	Column position	m

Subscripts

Variable	Description
act	actual
alk	alkalinity
i	component
liq	Liquid phase
T	total
vap	Vapour phase

Superscripts

Variable	Description
exp	Experimental value
In	Inlet stream
Out	Outlet stream
Sim	Simulated value

Greek letters

λ	Latent heat of vaporization	kJ/kg

1 Introduction

Carbon dioxide is a naturally occurring chemical compound that exists in Earth's atmosphere as a trace gas. CO_2 is essential to the existence of life on Earth since it is one of the key compounds in photosynthesis, the process by which plants and other organisms convert solar energy into chemical energy. Also, being a greenhouse gas it has major influence in the reflection of solar radiation back to Earth, keeping the planet's surface temperature suitable to the existence of life. CO_2 concentration in atmosphere used to be regulated by photosynthetic organisms, however since the industrial revolution it has greatly increased, becoming the major greenhouse gas that contributes to global warming – more than 60% (Wu et al. 2014). Carbon dioxide is released by the combustion of fossil fuels such as coal, natural gas and oil, by biomass as a fuel, and by certain industrial processes. Electrical-power generation remains the single largest source of CO_2 emissions, being responsible for 42% of the worldwide emissions (Agency, International Energy 2013a, Boot-Handford et al. 2014).

According to Cuéller-Franca and Azapagic (2015) global emissions of CO_2 from fossil fuels are now 60 % above 1990 levels. Also, according to the 2013a International Energy Agency report in the first ten years of the 21st century, the worldwide CO_2 emissions from fossil fuel combustion increased by 31%, reaching a value of 31 billion tonnes per year. The IPCC special report, 2005, presented four technological options to reduce anthropogenic emissions of CO_2:

1. Reduce the use of fossil fuels by improving the efficiency of energy conversion, transport and end-use;
2. Switch to less carbon-intensive fuels instead of more carbon-intensive fuels (e.g. natural gas instead of coal);
3. Increase the use of renewable energy sources, which emits little or no net CO_2;
4. CO_2 Capture and Storage (CCS).

Carbon capture and storage technology involves capturing CO_2 produced by large industrial plants, compressing it for transportation and then injecting it deep into a rock formation at a carefully selected and safe site, where it is permanently stored. CCS technology can capture up to 95% of the carbon dioxide generated in power plants and some industrial processes, preventing its release to the atmosphere (Association, Carbon Capture and Storage, *online*).

Despite major developments in the renewable energy sector, fossil fuels still represent more than 80 % of the world's primary energy supply (Agency 2013b, Adegbulugbe et al. 2005, Wu et al. 2014) . Therefore, the implementation of CCS technology in power plants is one of the options that can enable the utilization of fossil fuels with lower CO_2 emissions, thus representing a significant step towards greenhouse gas emissions reduction.

Carbon capture technologies have been used at large-scale for decades in the natural gas and fertiliser industries and have recently become operational in the power sector (Institute, Global CCS, *online*).

At this point, despite being the most mature technology for the sequestration of CO_2 from power plants based on post-combustion capture (PCC) processes, solvent-based solutions have high operating costs and represent a significant decrease in net power generation, which are major barriers to full-scale implementation. For this reason a lot of research is being devoted to find new solvents and process configurations that could improve process efficiency and thus reduce its costs.

1.1 Motivation

Process Systems Enterprise Limited (PSE) is the world leading provider of advanced process modelling software and model-based engineering to the process industries. PSE's technology and services are applied in seven main sectors: Chemicals & Petrochemicals, Oil & Gas, Life Sciences, Food & Consumer Products, Fuel Cells & Batteries, Wastewater and Power & CCS.

In July 2014, the company launched the gCCS® modelling environment, being the first modelling software specifically designed for the modelling of full carbon capture and storage chains, covering CO_2 capture, compression, transport and injection (PSE 2014b).

gCCS® is constructed on PSE's platform for advanced modelling, gPROMS®, allowing the use of high-fidelity predictive models. Using the gCCS® model libraries, it is possible to simulate each stage of the CCS chain individually and to analyse the interoperability across different chain components. Shell's Peterhead CCS project is the first commercial application of gCCS® in the United Kingdom, where it is being used to provide insight into the transient behaviour of the amine-based capture unit, and its effect on operations when integrated in the full CCS chain (PSE 2014a).

The gCCS® capture library contains models for the simulation of both chemical and physical solvent-based pre and post-combustion capture units. For rigorous physical properties estimation, these models use gSAFT, a thermodynamic property package created by PSE, which is based on the Statistical Association of Fluid Theory (SAFT) developed at Imperial College London.

The main goal of this thesis is to apply gPROMS® flowsheeting and optimisation features to model and compare different process configuration solutions for the removal of CO_2 from flue gases employing Piperazine as a solvent, using the gCCS® capture library.

1.2 Original contributions

Several processes and flowsheets have been previously assembled on gPROMS® regarding chemical solvent-based CO_2 capture using the solvents available: monoethanolamine, methyldiethanolamine activated with piperazine, and ammonia. This work improved the gCCS® library adding piperazine as a solvent and testing it for different flowsheet configurations.

The present thesis intends to understand and compare the effects of different flowsheet configurations on CO_2 capture results, especially regarding energetic consumption, which is the main obstacle to overcome.

1.3 Dissertation outline

This thesis is organised in the following way: Chapter 2 presents a literature review on CO_2 capture technologies, in which chemical solvent-based post-combustion capture with amines is further analysed. Chapter 3 features a brief description of gPROMS® ModelBuilder, the required models from gCCS® capture library and their initialisation procedure, the used physical properties package (gSAFT), and the transport properties of piperazine that had to be added to the models. Chapter 4 describes the validation of the models used for flowsheeting, which was achieved by the comparison of simulation results with experimental data publically available. Chapter 5 features the results and the comparison of the piperazine capture plant models assembled on gPROMS®. Chapter 6 presents a sensitivity analysis regarding several key variables and the optimisation results of three configurations using gPROMS® optimisation tool. Chapter 7 contains the conclusions drawn from this thesis and future work suggestions.

2 Background

A literature review was conducted in order to understand the basic concepts associated with CO_2 capture, particularly the existing post-combustion chemical solvent-based technologies.

2.1 Carbon Capture and Storage

The CCS chain comprises three essential stages: capture, transport and safe storage of CO_2. This technology can be applied to large-scale emission processes, including coal and gas-fired power generation and to some chemical industries such as cement, iron and steel, and paper (Institute, Global CCS, *online*).

The capture stage involves the processes required for the removal of CO_2 from a mixture of gases produced at large industrial facilities. The obtained CO_2 stream is then compressed and readily transported to the safe storage site. The transportation can be carried out via pipelines, ships or road tankers. The final stage consists in the injection and storage in an appropriated storage location, which may be underground rock formations or the deep ocean. The injection technology is similar to the one employed in the oil and gas industries, and can be associated with enhanced oil recovery (EOR), thus constituting a possible revenue source. Besides storage, in the past years the captured CO_2 has been considered for the production of other chemical, mineral fixation and the production of biofuels through the use of micro-algae (Institute, Global Carbon Capture and Storage, *online*).

The world's first large-scale CCS project applied to the power sector started its operation in October 2014 at the Boundary Dam power station in Saskatchewan, Canada. Post-combustion amine-based CCS technology was implemented to a coal-fired power plant more than half a century old, being the captured CO_2 used for EOR. In February 11, 2015, SaskPower released preliminary numbers for the operation of the station and the CCS performance is exceeding expectations. The power plant is generating 120 MW (10 MW over the predictions) and 1 Mt of CO_2 per year is being captured, with 99.9 % purity. CO_2 emissions were reduced from 1.1 Mt to 100 000 t per year, which represents a CO_2 capture of almost 91 % (SaskPower 2015).

Two additional large-scale CCS projects in the power sector are planned to start operating: the Kemper County Energy Facility in Mississippi and the Petra Nova Carbon Capture Project in Texas.

Kemper County's predicted start-up date was May 2015 but no information has yet been released regarding its operation or performance. The 3.5 Mt of CO_2 captured annually (65 % of the total produced) through pre-combustion Integrated Gasification Combined Cycle (IGCC) technology will be transported via pipelines and used for EOR (MIT 2015a).

Petra Nova Carbon Capture Project is scheduled to start at the end of 2016. The existing coal-fired power plant will be retrofitted to capture 1.4 Mt/year, which corresponds to 90 % of the produced carbon dioxide. It will use the KM-CDR amine scrubbing process developed by Mitsubishi Heavy Industries and Kansai Electric Power Company (MIT 2015b).

2.2 Carbon Capture Technologies

The main technologies available for CO_2 separation and capture are shown in Figure 2.1.

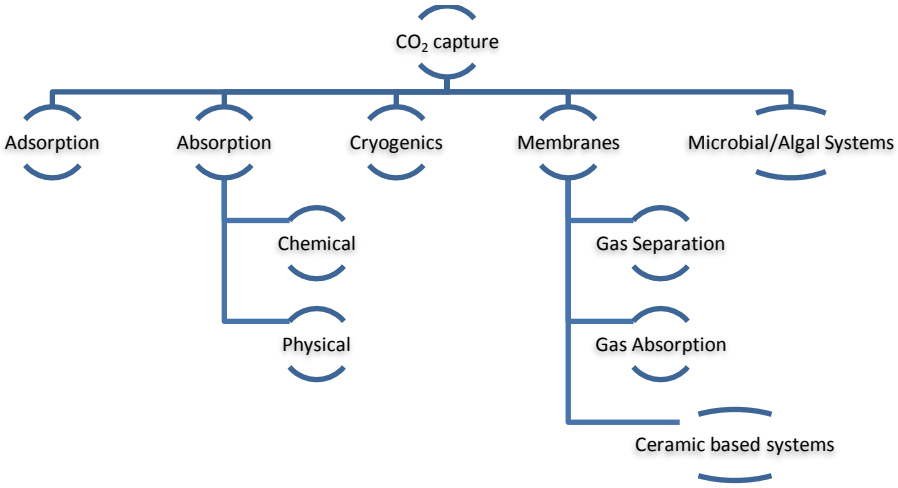

Figure 2.1 – Available technologies for CO_2 capture (Rao and Rubin 2002).

There are three major approaches for Carbon Capture and Storage: post-combustion capture, pre-combustion capture and oxy combustion capture.

Both post-combustion and pre-combustion carbon capture technologies are economically feasible under specific conditions while oxy-fuel combustion is still under demonstration. Currently available technology is capable of capturing about 85-95% of the CO_2 processed in a capture plant (Adegbulugbe et al. 2005). For power plants, the technology employed in the capture process depends on the characteristics of the gas being treated, so it will vary with the fuel and technology used for energy production.

This literature review focuses on chemical absorption associated to the post-combustion capture approach. The other technologies and CCS approaches are briefly described in Appendix 1.

PCC involves the separation of CO_2 from the flue gases produced by the combustion of fossil fuels – coal, oil or natural gas – in power plants with air (Institute, Global CCS 2012b) and from the waste gas streams resulting from the production of ethylene oxide, cement and biogas sweetening (Cuéllar-Franca and Azapagic 2015).

This technology can be divided in three categories: biological, physical and chemical methods. Biological method refers to CO_2 fixation by photosynthesis of plants, algae and

photosynthetic bacteria without energy consumption. Physical methods involve CO_2 absorption and removal with organic solutions without chemical reaction. As to chemical method, CO_2 is removed by reacting with chemical compounds. The chemical method includes chemical adsorption, chemical looping combustion and chemical absorption (Boot-Handford et al. 2014).

In a typical power plant the fuel is combusted with air for steam generation, which is then used for the production of electricity in a steam turbine. A schematic representation of the PCC process is presented in Figure 2.2.

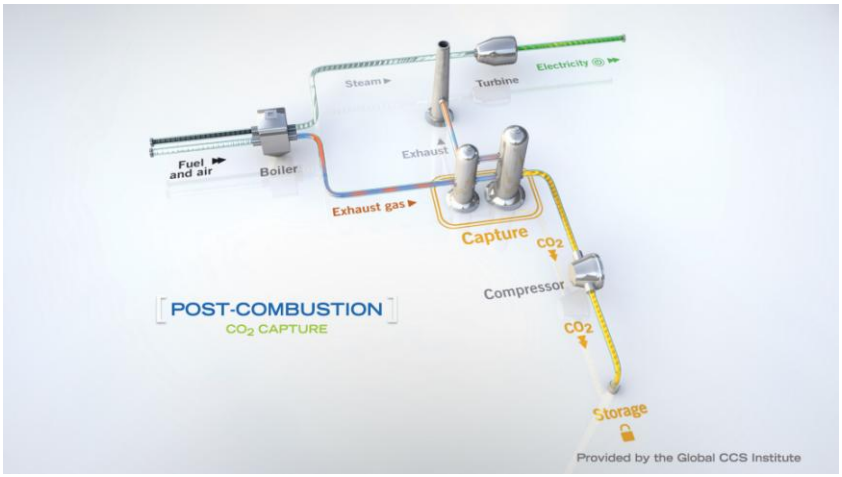

*Figure 2.2 - Schematic representation of a power plant with post-combustion CO_2 capture (*Institute, Global CCS, *online).*

The flue gas exiting the boiler has high content of nitrogen and low content of carbon dioxide, water and oxygen, at pressure close to atmospheric. It also contains small amounts of impurities such as SO_x, NO_x and ash that must be removed before the capture process through electrostatic precipitation and desulphurization (Boot-Handford et al. 2014).

The typical concentration of each specie in the flue gas obtained from the combustion of coal and natural gas is presented in Table 2.1.

Table 2.1 - Typical composition of flue gas from coal and gas fired power plants (Institute January 2012b).

Gas constituent	Composition (vol. %)	
	Coal	Natural Gas
N_2	70-75	73-76
CO_2	10-15	4-5
H_2O	8-15	8-10
O_2	3-4	12-15
Trace gases	<1	<1

Post-combustion CO_2 capture can be accomplished by means of chemical solvents, membranes, solid sorbents, or by cryogenic separation, among others. Nevertheless, chemical absorption with amine-based solvents is currently the state-of-the-art technology for post combustion carbon capture (Wu et al. 2014) and according to Global CCS Institute report on post-combustion capture, 2012, the technologies currently tested on pilot plants are universally based on absorption with aqueous solvents.

Absorption processes allow CO_2 capture rates up to 95 %, and purity as high as 99.9 vol.% for the recovered CO_2 (Adegbulugbe et al. 2005). Since the stream being treated is at nearly atmospheric pressure and has low CO_2 content, the CO_2 partial pressure is reduced. Therefore the chosen solvent has to be able to ensure acceptable loadings (the ratio of the number of mole of CO_2 and amine) and kinetics in the referred conditions. Due to this, chemical absorption poses a better option in PCC processes, when compared with physical solvents.

PCC offers some advantages as it can be applied to newly designed facilities or implemented as a retrofit option to existing power plants without radical changes on them (Wu et al. 2014).

2.3 Chemical solvent-based Carbon Capture Processes

Chemical absorption, also known as gas scrubbing, is based on the reaction of CO_2 with an alkaline solvent to form a weakly bonded intermediate compound which may be regenerated with the application of heat or the decrease of pressure, producing the original solvent and a CO_2 stream. The selectivity of this form of separation is relatively high, particularly when using amines as solvent. In addition, a relatively pure CO_2 stream could be produced. These factors make chemical absorption well suited for CO_2 capture of industrial flue gases (Wang et al. 2011).

Chemical absorption/stripping for CO_2 separation is a mature technology that was first patented in the 1930s (Dugas and Rochelle 2011b) and has been widely used in the chemical industry, being currently considered the most viable option and the technology of choice for carbon capture from coal-fired power plants (Rochelle et al. 2011). Post and pre-combustion capture at lower CO_2 partial pressures are mainly based on this technology.

The selection of the solvent depends on the conditions of the gas being treated: its pressure, temperature, CO_2 composition and impurities present. Gas characteristics also determine process variables as temperature, pressure and flow rates, construction materials, use of inhibitors and equipment design and configuration (Plaza 2012). A good solvent for CO_2

capture has high CO_2 absorption rate, CO_2 capacity and resistance to degradation, and low volatility and corrosiveness (Singh, Swaaij, and Brilman 2013b, Salazar et al. 2013).

Higher solvent concentrations lead to a reduction of the equipment size and process thermal and pumping requirements due to the solvent flow rate reduction so it is important to keep it as elevated as possible. Nevertheless, due to amines reactivity they are highly prone to oxidative and thermal degradation, which limits its concentration (Singh, Swaaij, and Brilman 2013a).

Most representative solvents that are being considered for chemical-based carbon capture are alkanolamines, ammonia, amino-acid salts and hot potassium carbonate.

A conventional flowsheet for a PCC plant operating with chemical absorption is shown in Figure 2.3.

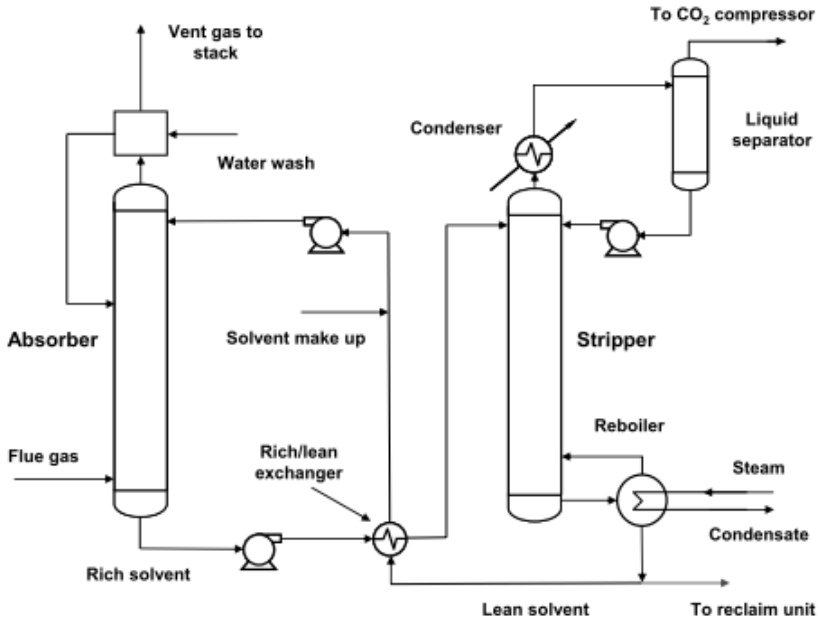

Figure 2.3 - Process flow diagram for CO_2 capture by chemical absorption (EPRI November 2005).

Prior to absorption, other acid gases such as SO_2 and NO_2 must be removed since they affect the performance of the system by forming heat stable salts with the solvent. SO_2 required concentration lower than 10 ppm can be achieved through flue gas desulphurization; NO_x concentration is reduced by selective catalytic reduction, selective non-catalytic reduction or low NO_x burners. Particulate matter such as fly ash can be eliminated in electrostatic precipitators (Cousins, Wardhaugh, and Feron 2011).

Flue gases from a combustion power plant are usually above 100 ^oC, thus in order to minimize solvent degradation and improve CO_2 absorption they must be cooled to a temperature lower than 65 ^oC (EPRI November 2005) in a direct contact cooler, and are then sent to the absorber.

During the chemical absorption process the cooled flue gas enters a packed bed absorber which is at temperatures typically between 40 and 60 ^oC from the bottom and counter-currently contacts with the aqueous solvent. The lean solvent gradually heats up as CO_2 diffuses from the gas into the liquid film. The scrubbed gas may be water washed or directly vented to the atmosphere, depending on the amount of solvent on that stream.

After leaving the absorber, the rich solvent is heated in a cross exchanger by regenerated hot-lean solvent from the stripper's reboiler. It then flows into the top of the stripper where it is regenerated at elevated temperatures (100-150 ^oC) and at pressures in the range of 1.5-2 atm. Heat is supplied by the reboiler, which is the major energy penalty of the process. After solvent regeneration the CO_2 lean solvent is pumped back to the absorber via the cross heat exchanger to reduce the temperature (Wang et al. 2011). The pure CO_2 released from the top of stripper is then compressed for the subsequent transportation and storage.

The industry standard for chemical solvent-based carbon capture is monoethanolamine (MEA) due to its low cost and high capacity, heat of absorption and rates of reaction. However, in order to reduce energy penalty and improve process performance, other options have been studied in the past few years, such as the alkanolamines diethanolamine (DEA), diisopropanolamine (DIPA), methyldiethanolamine (MDEA) and piperazine (PZ), ammonia and potassium carbonate. More recently, there has been growing interest in using improved and activated solvents, mixing amines to capitalize the advantages of each one of them: combine the higher reaction rate of primary/secondary amines with the higher equilibrium capacity of the tertiary/sterically hindered amines, leading to significant saving in process costs. This blends present enhanced absorption performance due to the presence of the primary/secondary amine and low energy consumption for the solvent regeneration due to the tertiary/hindered amine (Closmann, Nguyen, and Rochelle 2009).

2.3.1 Amine-based capture processes

Aqueous alkanolamine solutions are widely used for the removal of acid gas impurities such as carbon dioxide and hydrogen sulphide from natural gas, hydrogen and synthesis gas for ammonia production (Samanta and Bandyopadhyay 2007, Fu, Li, and Liu 2014).

Amine nomenclature is based on the number of carbon atoms in the amine group. Primary (e.g. MEA), secondary (e.g. DEA, DIPA) and tertiary (e.g. MDEA) amines have one, two and three carbon groups connected to the amine group, respectively, as can be seen in Figure 2.4.

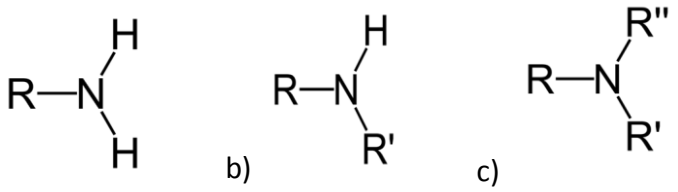

Figure 2.4 – Schematic representation of a) primary, b) secondary and c) tertiary amines.

Due to the presence of at least one hydrogen atom, primary and secondary amines react strongly and at elevated reaction rates with CO_2, even at low partial pressures. However they have high volatility and require oxidation inhibitors due to corrosion and degradation problems (Dubois and Thomas 2013).

Tertiary and hindered amines provide higher CO_2 loadings and have lower energy requirements. Nevertheless, they have considerably slower kinetics, thus requiring the use of promoters (Dubois and Thomas 2013).

Sterically hindered amines are primary or secondary amines that were modified so that the carbon atom bounded to the amine group is secondary or tertiary, thus reducing its reactivity. Examples of these amines are 2-amino-2-methyl-1-propanol and 2-piperidineethanol (Vaidya and Kenig 2007).

Primary and secondary amines ($RR'NH$) react with CO_2 producing a compound called carbamate ($RR'NCOO^-$) through the formation of an intermediate zwitterion ($RR'NH^+COO^-$), which correspons to the mechanism's slow step (Thee et al. 2012). The mechanism can be represented by equations 2.1 and 2.2.

Besides these reactions, CO_2 is also converted into bicarbonate through the reaction described in equation 2.3. Nevertheless, for loadings below 0.5 mol_{CO2}/mol_{alk}, the bicarbonate formation can be considered insignificant when compared to the carbamate formation (Khan, Krishnamoorthi, and Mahmud 2011).

$$CO_2 + RR'NH \rightleftarrows RR'NH^+COO^- \quad (2.1)$$

$$RR'NH^+COO^- + RR'NH \rightleftarrows RR'NCOO^- + RR'NH_2{}^+ \quad (2.2)$$

$$CO_2 + RR'NH + H_2O \rightleftarrows HCO_3{}^- + \ RR'NH_2{}^+ \quad (2.3)$$

Hindered amines form a carbamate of low stability due to the large group connected to the amine group. This unstable carbamate is hydrolysed originating a bicarbonate ion (Vaidya and Kenig 2007).

$$RR'NCOO^- + H_2O \rightleftarrows HCO_3{}^- + RR'NH \quad (2.4)$$

Combining equations 2.1, 2.2 and 2.4 it can be observed that for hindered amines the global reaction is equivalent to the reaction described in equation 2.3, being the reaction

stoichiometry of 1:1 between CO_2 and the amine. In the case of un-hindered amines, the global stoichiometry is 1:2. This difference in the global stoichiometry leads to a maximum loading of 0.5 mol_{CO2}/mol_{alk} for unhindered amines, while hindered amines present a maximum loading of 1 mol_{CO2}/mol_{alk} (Vaidya and Kenig 2007).

Tertiary amines ($RR'R''N$) do not have hydrogen atoms bounded to the amine group, so they are not able to react directly with CO_2. Relevant reactions for this type of amines are presented in equations 2.5 and 2.6.

$$CO_2 + OH^- \rightleftarrows HCO_3^- \quad (2.5)$$

$$RR'R''N + H_2O \rightleftarrows RR'R''NH^+ + OH^- \quad (2.6)$$

The limiting step for this mechanism is the CO_2 hydrolysis, therefrom the reduced reaction rate.

2.3.2 Piperazine as the new benchmark solvent

Piperazine is a cyclic diamine with two secondary amine nitrogen atoms, which provide large reactivity and CO_2 capacity (Bishnoi and Rochelle 2000). Its cyclic structure exposes the nitrogen groups and results in very fast reaction with CO_2. The ring structure also provides increased resistance against thermal degradation allowing for stripping at higher temperatures.

PZ has been used as an effective promoter to increase absorption rates and capacity in solvents such as K_2CO_3, MEA and with MDEA for over almost 30 years (Plaza and Rochelle 2011, Freeman et al. 2010, Muhammad et al. 2009). PZ has been found to be a good promoter compared to other amines because it leads to higher rates of absorption while maintaining a low heat of regeneration in the stripper section (Moioli and Pellegrini 2015b). As a promoter, PZ concentration is low due to its low solubility: between 0.5 and 2.5 molal (m).

PZ is used as an activator in the BASF's activated MDEA (aMDEA) technology for natural gas sweetening and it is reported to be more effective than the conventional rate accelerators (Samanta and Bandyopadhyay 2007). The blend MDEA/PZ takes advantage of the relatively high heat of reaction of CO_2 with the activating agent combined with the benefits of high loading capacity of MDEA and relatively low cost of regeneration of the activated solvent.

Piperazine is nearly ten times more reactive than any of the other presented amines. Due to these characteristics, PZ reacts rapidly with CO_2 as soon as the gas dissolves into the liquid. It then shuttles the CO_2 (as carbamate) into the interior of the liquid where it dissociates back into the free amine and transfers the CO_2 to the activated solvent. The promoter diffuses back to the interface for more CO_2 (Contactor 2008).

Regarding the piperazine system, the relevant reactions are described in equations 2.7-2.10 (Sachde and Rochelle 2014).

$$2\,PZ + CO_2 \rightleftarrows PZH^+ + PZCOO^- \tag{2.7}$$

$$2\,PZCOO^- + CO_2 \rightleftarrows PZ(COO)_2{}^{2-} + H^+PZCOO^- \tag{2.8}$$

$$PZCOO^- + CO_2 + H_2O \rightleftarrows HCO_3{}^- + H^+PZCOO^- \tag{2.9}$$

$$PZ + H^+PZCOO^- \rightleftarrows\ PZH^+ + PZCOO^- \tag{2.10}$$

The second order reaction rate constants at 25 °C for the amines previously mentioned are listed in Table 2.2.

Table 2.2 - Reaction Rate Constants of commonly used amines with CO_2 (Contactor 2008).

Amine	Reaction rate constant $(\mathbf{L \cdot mol^{-1} \cdot s^{-1}})$
MEA	6000
DEA	1300
DIPA	100
PZ	59000
MDEA	4

30 wt. % (7 molal) MEA has been the standard solvent for the evaluation of processes for post-combustion CO_2 capture. However in the past few years, concentrated aqueous PZ has been investigated as a novel amine solvent for CO_2 capture and has shown good potential, so it is now being proposed as the new benchmark by the research community (Rochelle et al. 2011).

Although pure PZ boiling point (146 °C) is lower than that for MEA (171 °C), the volatility of high concentration PZ (>5 m) is similar to MEA's because of its low activity coefficient in water (Rochelle et al. 2011, Hilliard 2008). Nevertheless, PZ provides CO_2 absorption rate 2-3 times faster (Dugas and Rochelle 2009, Freeman et al. 2010) and better capacity – near double of that of 7 m MEA (Chen et al. 2014). PZ also has moderately high heat of absorption (≈70 kJ/mol) (Kim and Svendsen 2011) and very good resistance to oxidative and thermal degradation so it can be used up to 150 °C (Mazari et al. 2014), which should provide 10-20 % better energy performance (Plaza and Rochelle 2011, Freeman et al. 2010). Also, studies indicate that 8 m PZ decreases the total equivalent work requirement of the simple stripper and two-stage flash configurations by 7.8 and 4.2%, respectively, when used instead of 9 m MEA (Van Wagener and Rochelle 2011, Van Wagener, Rochelle, and Chen 2013).

8 m PZ process limitations are related to the solubility issues encountered at both lean and rich CO_2 loadings, since its melting point is very high (106 °C), leading to a limited operating range (Chen et al. 2014, Dugas and Rochelle 2011a, Moioli and Pellegrini 2015a).

2.3.3 Pilot plant studies with piperazine

Most studies related to post-combustion CO_2 capture with piperazine are being conducted at the University of Texas at Austin (Seibert et al. 2011). Since 2008, five pilot plant campaigns were carried out, being their conditions summarized on Table 2.3.

Table 2.3 - Pilot plant campaigns conditions (Sachde, Chen, and Rochelle 2013).

Pilot plant campaigns	November 2008	September 2010	December 2010	October 2011	November 2013
Piperazine concentration	5 - 9 m	8 m	8 m	8 m	3.6-3.75 m
Packing	Structured 2X	Hybrid 250	Hybrid 250	Structured 350 Z	Hybrid 250Y
Gas rate (ft_{act}^3/min)	350	250-750	350-650	360-675	360
Liquid rate (gallon/min)	12-18	8-26	8-26	11-22	12
Intercooling	No	Yes/No	Yes	Yes (with spray)	Yes/No

In November 2008 the simple absorber and simple stripper configuration shown in Figure 2.5 was implemented. Inlet temperatures on the absorber were kept at 40 °C, for both flue gas and lean solvent. The stripping process occurred at 1.38 bar and 128 °C, throughout fifteen non-equal runs, resulting in capture rates between 48.7 and 93.2 % (Plaza and Rochelle 2011).

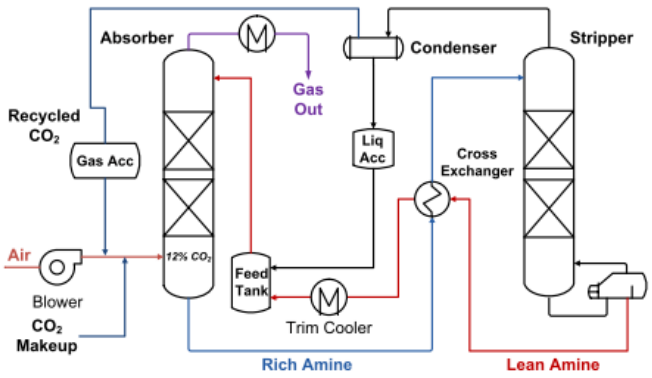

Figure 2.5 - November 2008 Pilot Plant Campaign (Plaza 2012).

In September and December 2010 intercooling was retrofitted to the existing absorber column, as shown in Figure 2.6 (Van Wagener, Rochelle, and Chen 2013). For this configuration, stripper temperature was slightly decreased to 120 °C.

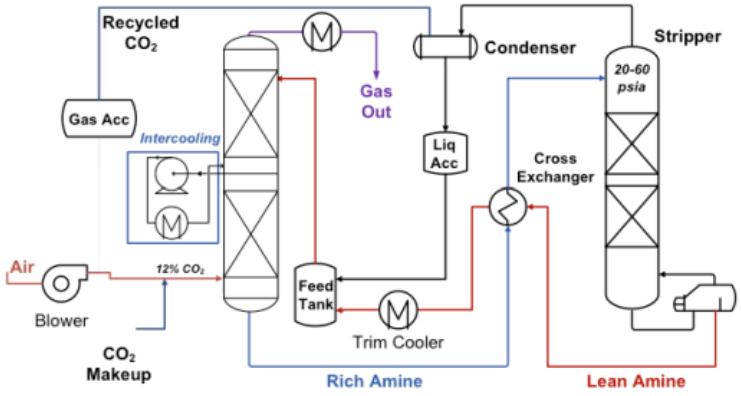

Figure 2.6 - September and December 2010 Pilot Plant Campaign (Plaza 2012).

In October 2011 the simple stripper was replaced for a two-stage flash that can be seen in Figure 2.7. It allowed to evaluate CO_2 regeneration at higher temperature and pressure (150 °C and 14 bar) (Walters et al. 2013, Madan et al. 2013, Chen et al. 2013, Sachde, Chen, and Rochelle 2013).

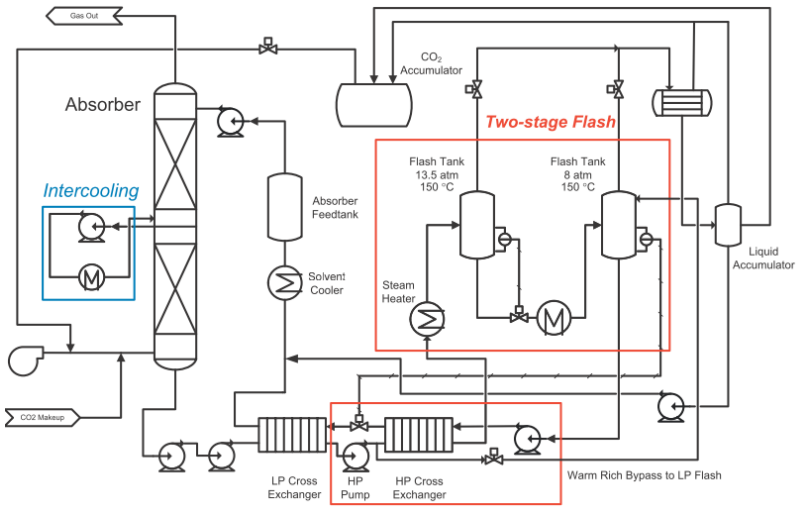

Figure 2.7 - October 2011 Pilot Plant Campaign (Plaza 2012).

In this configuration the rich solvent exiting the main cross-exchanger is delivered to a second, high-pressure, heat exchanger to attain the temperature on the flash vessels, higher than the typical campaigns with the simple stripper.

In December 2011, a cold rich bypass was added to the low pressure flash vessel. Bypass flowrate was 10 % of the total volumetric flow leaving the absorber column (Figure 2.8) (Madan et al. 2013).

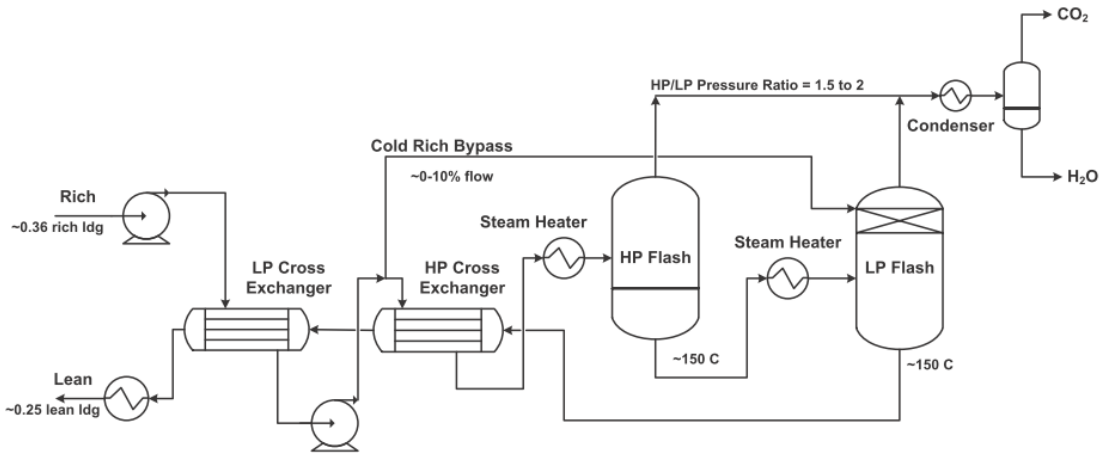

Figure 2.8 - December 2011 Pilot Plant Campaign (Madan et al. 2013).

5 runs were carried out on December 2013 campaign with the goal of developing methods for generating, measuring and capturing PZ aerosols (Chen et al. 2014).

3.7 m PZ was used in order to eliminate the solubility limitation on the rich CO_2 loading end and expand the lean solubility window relatively to 8 m PZ.

The configuration that is shown in Figure 2.9 comprises an intercooled absorber and a single-stage high temperature flash with cold rich bypass, operated at 140 °C and 4.5 bar.

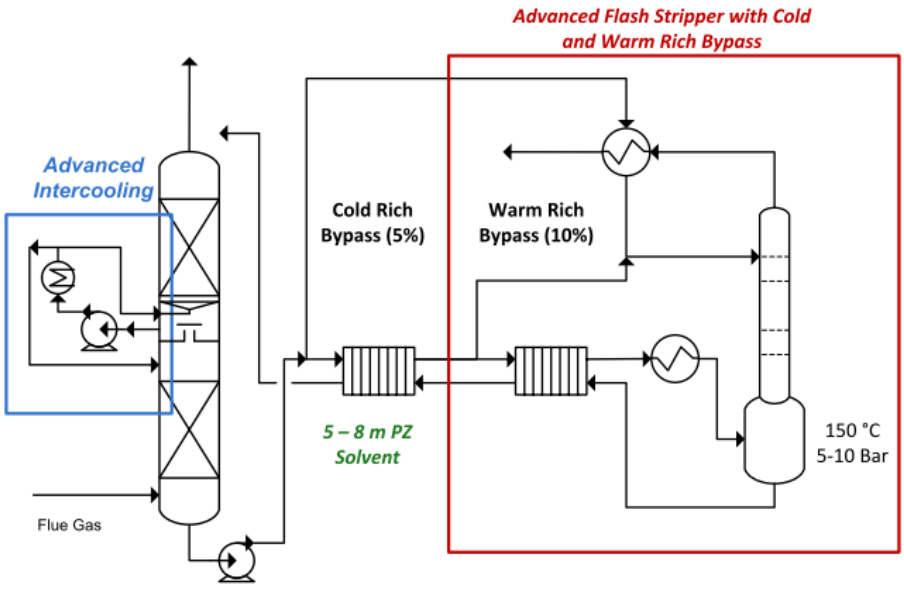

Figure 2.9 - November 2013 Pilot Plant Campaign (Chen et al. 2014).

3 Materials, Methods and Properties

3.1 gPROMS® ModelBuilder

gPROMS® ModelBuilder 4.1.0 is the simulation platform used for flowsheet model simulation and optimisation throughout the present thesis. This advanced modelling tool can be used for the development, validation, execution and deployment of models, using fast and robust numerical solvers (PSE 2015a).

A flowsheet can be assembled through a drag and drop system in the topology tab of a model entity, starting from an existing model library, such as the gCCS® library. This way, a new model is built, being composed by the models retrieved from the library and the respective connections. Furthermore, in the gPROMS® language tab of the same model, it is possible to include any other auxiliary equations and custom sub models. Through the inclusion of the created model on a process entity, its simulation can be achieved.

gPROMS® ModelBuilder optimisation tool can be used to optimise the steady state and/or dynamic behaviour of a continuous flowsheet, considering both design and operation properties. The optimisation procedure acts on a specified process and requires the indication of the unassigned variables acting as objective function or process constraints and the assigned variables, which work as decision/control variables.

3.2 gCCS® Capture Library Models

gCCS® is a tool to support the design and operating decisions across the CCS chain. The gCCS® libraries contain steady-state and dynamic models for all the major operations, from power generation through capture, compression and transmission to injection, and can be used either for modelling individual systems or to study the interoperability across the CCS chain components (Rodriguez et al. 2013).

Absorber and stripper columns can be modelled using two different approaches: equilibrium-based or rate-based. Equilibrium-based is good enough for physical absorption models but not for chemical ones, since for this case the state of equilibrium is rarely attained (Wang et al. 2011). The rate-based approach comprises chemical reactions and multi-component mass and heat transfer correlations, and is the one used on gCCS® models (Rodriguez et al. 2013).

The absorption/desorption units are based on the two film-theory and are distributed in the axial direction – the vapour and liquid films are not discretized, and the reactions are treated implicitly and assumed to occur only in the liquid bulk (Wang et al. 2011, Kenig, Kucka, and Gorak 2003, Rodriguez et al. 2013). It is also assumed phase and chemical equilibrium at the

interface. The mass transfer coefficients for both phases, pressure drop, loading and flooding limits, liquid holdups and interfacial area are calculated with suitable correlations, which can be specified by the user (Rodriguez et al. 2013).

Absorption systems often contain molecular and electrolyte species and thus are characterized by highly non-ideal behaviour. An appropriate thermodynamic model is necessary for the accurate calculation of thermodynamic equilibrium at the phase interface. Therefore, instead of using typical models for systems containing electrolytes with a chemical approach such as Pitzer, Electrolyte NRTL or UNIQUAC, which require knowing reaction products and mechanisms a priori (Kenig, Kucka, and Gorak 2003, Dowell et al. 2011), these models are based on rigorous gSAFT physical properties.

The high-fidelity models utilised for the simulation of a chemical-based post-combustion capture unit throughout the present thesis are briefly described in Appendix 2.

3.3 Models Initialisation

Some models in the gCCS® libraries include an *Initialisation Procedure*. Briefly, this automatic procedure starts the calculations considering the simplest situation and assumptions for each model and sequentially, in a certain number of steps, increase the level of complexity until the final solution is obtained.

Absorber, stripper and flash drum models are not able to initialise for every set of conditions. In fact, when using piperazine as a solvent, these models only initialise for a specific range of conditions, which are very different from the operating ones. This makes the initialisation one of the most time-consuming processes of the whole flowsheeting part.

First of all the model has to be initialised using its *Initialisation Procedure*, with some specific conditions that are obtained by a trial and error process. Once it converges and a solution is calculated, its Variable Set, which is a file that contains all the values calculated, must be saved in the *Saved Variable Sets* folder.

From that point onwards, the Variable Set saved must be restored and the Initialisation Procedure ignored. Input conditions of the model are then changed gradually until the desired values are reached.

If the alterations made on the input are small enough, it is possible to obtain a solution.

3.4 Physical Properties Package – gSAFT

gSAFT is a physical properties package developed and commercialised by PSE that implements the SAFT technology to model the behaviour of the liquid and gas mixtures. This technology uses the Statistical Associating Fluid Theory equation of state developed at Imperial College

London, an advanced molecular thermodynamic method that is based on statistical mechanics and has a limited number of parameters with a clear physical meaning. Hence, these parameters can be fitted to a limited amount of experimental data and used to predict phase behaviour and physical properties for a wide range of conditions, being able to model complex mixtures of associated fluids (PSE 2015b, Rodriguez et al. 2013). SAFT equation of state can predict a wide variety of thermodynamic properties of mixtures accurately, based in physically-realistic models of molecules and their interactions with other molecules. Thus, the reaction products are modelled as aggregates of the reactants, without explicitly treating the formation of new species, by assuming chemical equilibrium everywhere across the film and the bulk liquid regions.

The assumption of chemical equilibrium is only valid when the mass transfer rate is slow compared to the reaction kinetics (the mass transfer is limited by diffusion). This is true for MEA (Rodriguez et al. 2013) hence also for PZ, which has higher reaction kinetics.

In these models it is taken into account the shape, size and specific interactions between the existing molecules in a mixture, which are considered as chains of spherical segments, so the reaction products are modelled as aggregates of the reactants. This is particularly relevant when considering non-spherical molecules with strong directional interactions, such as the hydrogen bounds in PZ-based solvent.

gSAFT package used in the models presented in this thesis is based on the equations of state SAFT-VR, according to which the attraction/repulsion between segments or molecules is modelled using the "square-well" potential energy function. This function is characterised by the diameter of the segment, the range of dispersion interactions and its strength. The physical basis of these parameters allows its systematic use to describe similar molecules or predict physical properties in a wide range of conditions (PSE 2015b, Dowell et al. 2011). It requires the specification of some non-equilibrium physical properties such as diffusion coefficients, viscosities and surface tensions (Kenig, Kucka, and Gorak 2003).

For carbon capture gSAFT presents a modelling alternative to phase and chemical equilibrium in the CO_2-PZ-H_2O system. Using the gSAFT equation of state the chemical bond between CO_2 and PZ can be incorporated as a short-range association, being included in the molecular model. This way, only reactants are considered and the involved reactions are treated implicitly, thus greatly reducing the complexity of the model and increasing its robustness.

Throughout this thesis, the thermodynamic properties are calculated with gSAFT.

3.5 Transport properties of Piperazine

Although the models previously mentioned already existed in gCCS® capture library, the only solvents for which there were already information regarding their transport properties were MEA, MDEA, activated MDEA (aMDEA) and NH_3. Therefore, correlations for some transport properties of piperazine had to be incorporated into the existing gCCS® models.

A sensitivity analysis was made to analyse the effect of surface tension value on the results, since there is limited information available regarding this parameter. According to the results obtained, surface tension doesn't significantly affect the results, so the value considered was the same as for aMDEA, which is a blend of piperazine and MDEA.

According to the literature, diffusivity coefficient values are greater for PZ than for MEA but once again there is little experimental data available. Therefore its values were adjusted so the results approached the experimental data.

PZ viscosity is ten times larger than that for MEA in the operating range of temperatures. According to experimental data, its value depends on the solvent concentration, CO_2 loading and temperature (Moioli and Pellegrini 2015b, Derks et al. 2008, Derks, Hogendoorn, and Versteeg 2005). Since PZ concentration as a solvent is always near 8 m and the loading doesn't significantly affect the results (as can be seen in Figure 3.1), the correlation that has been built based on Freeman (Freeman 2008) data is only function of temperature and corresponds to a CO_2 loading of 0.291, which is the middle one.

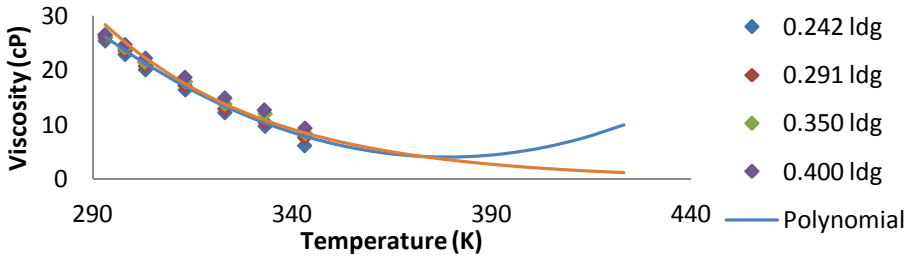

Figure 3.1 - Viscosity correlation as a function of temperature.

There is no available data for temperatures above 70 °C and as referred before, the stripping process can occur up to 150 °C (423 K). When using a polynomial equation and extrapolating values, for temperatures above 110 °C the viscosity values start increasing, which doesn't make sense physically.

For that reason, the correlation being used is the exponential equation represented in Figure 3.1:

$$Viscosity\ (\mathrm{cP}) = 32305 \times e^{-0.027 \times T(\mathrm{K})} \tag{3.1}$$

Although the equation used is based on 8 m PZ data, the results are not affected in a wide range of concentrations, as will be seen in Section 4.1.

4 Models validation

The validation of the absorber models was achieved through the comparison of the simulation results with experimental data publically available obtained from pilot plant campaigns conducted at the University of Texas at Austin.

4.1. Absorber model validation

Plaza and Rochelle, 2011, presented data obtained from a one month pilot plant campaign conducted in November 2008 at the University of Texas at Austin. The absorber model built on gPROMS® that is shown in Figure 4.1 was validated through the comparison of the referred data with the simulation results.

The presented data consists of fifteen runs with constant volumetric gas flow (around $0.165\ \mathrm{m^3/s}$ at $P = 1\ \mathrm{atm}$ and $T = 40\ ^{\circ}\mathrm{C}$) and CO_2 content around $12\ \%$. The pilot scale absorber has a diameter of $0.427\ \mathrm{m}$ and is packed with 6.1 m of Sulzer's packing Mellapak 2X divided into two equal beds.

Table 4.1 - Pilot plant conditions (Plaza and Rochelle 2011).

Run	PZ concentration (m)	L/G (mol L/ mol G)	Loading (mol CO_2/ mol alk)		Removal (%)
			Lean	Rich	
1	7.46	5.5	0.285	0.340	85.9
2	7.88	5.5	0.308	0.370	66.6
3	9.18	4.9	0.254	0.330	87.9
4	7.82	4.3	0.284	0.360	68.2
5	8.22	6.0	0.302	0.360	77.1
6	8.06	5.6	0.305	0.360	73.7
7	7.85	6.7	0.267	0.340	92.2
8	7.67	5.7	0.331	0.380	48.7
9	7.60	6.8	0.280	0.350	93.2
10	4.81	7.1	0.316	0.380	60.7
11	4.95	6.8	0.274	0.360	88.6
12	4.88	5.5	0.257	0.360	78.3
13	4.64	4.8	0.262	0.380	66.8
14	9	4.9	0.266	0.360	90.0
15	8	5.4	0.272	0.361	87.7

As can be seen in Figure 4.1, besides the absorber, source and sink models, the flowsheet includes a pump model without any specification before the absorber inlet in order to provide the required pressure for the liquid phase in the absorber model (A_001).

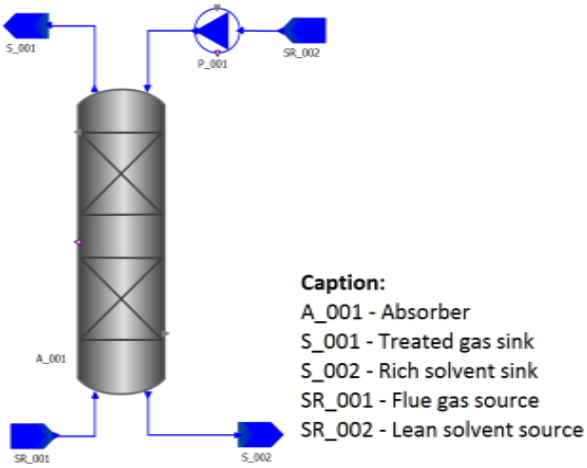

Figure 4.1 - Simple absorber model used for validation.

The lean solvent (SR_002) is introduced at the top of the column being the conditions used for the process simulation calculated with the inlet values presented in Table 4.1 and presented in Appendix 3. Amine concentration varied from 5 m to 9 m, with most data around 8 m.

The pilot plant absorber is fed at the bottom with a blend of nitrogen, oxygen, water and recycled CO_2 from the stripper, with CO_2 content around 12 % at constant flow rate (SR_002). Throughout the simulations the gas stream composition (SR_001) was assumed to be water saturated, with the characteristics shown in Table 4.2.

Table 4.2 - Flue gas composition.

Mass flowrate (kg/s)		0.1888
Mole fractions	H_2O	0.073
	CO_2	0.120
	N_2	0.757
	O_2	0.050
Temperature (°C)		40
Pressure (bar)		1.013

Since there is no available data regarding the packing used on the pilot plant tests, all fifteen runs were modelled using Sulzer's structured packing Mellapak 250Y™.

The parameters required to use Billet & Schultes correlation as mass transfer model with Sulzer's structured packing Mellapak 250Y™ already existed in the gCCS® models and can be found in Billet and Schultes, 1999.

The validation of the absorber model was based on the comparison of the CO_2 removal and the rich solvent loading, being these variables calculated through equations 4.1 and 4.2 using the mass fractions $(w_i{}^S)$, mole fractions $(x_i{}^S)$ and mass flow rates (F_S) of the treated gas (*TG*), flue gas (*FG*) and rich solvent (*RS*) streams .

$$CO_2\ removal\ (\%) = \left(1 - \frac{w_{CO2}{}^{TG} \cdot F^{TG}}{w_{CO2}{}^{FG} \cdot F^{FG}}\right) \times 100 \tag{4.1}$$

$$Rich\ loading\ (\mathrm{mol_{CO2}/mol_{alk}}) = \frac{x_{CO2}{}^{RS}}{x_{alk}{}^{RS}} = \frac{x_{CO2}{}^{RS}}{2\,x_{PZ}{}^{RS}} \tag{4.2}$$

The diffusivity coefficient of every solvent present in the gCCS® models is obtained by multiplying the value of 2×10^{-9} by a correction variable, which is different for each solvent. For piperazine, this variable was adjusted in order to minimise CO_2 removal deviations.

Table 4.3 shows the experimental data and simulation results along with the deviation between them, which is calculated through equation 4.3.

$$Deviation\ (\%) = \frac{v_i{}^{sim} - v_i{}^{exp}}{v_i{}^{exp}} \times 100 \tag{4.3}$$

Table 4.3 - Experimental and simulation results with a simple absorber.

Run	CO_2 removal (%)			Rich loading ($\mathrm{mol_{CO2}/mol_{alk}}$)		
	Experimental	Simulation	Deviation (%)	Experimental	Simulation	Deviation (%)
1	85.9	74.7	-13	0.340	0.358	5
2	66.6	61.7	-7	0.370	0.366	-1
3	87.9	92.5	5	0.330	0.340	3
4	68.2	65.7	-4	0.360	0.364	1
5	77.1	72.3	-6	0.360	0.361	0
6	73.7	66.0	-10	0.360	0.364	1
7	92.2	94.1	2	0.340	0.339	0
8	48.7	47.1	-3	0.380	0.376	-1
9	93.2	88.1	-6	0.350	0.349	0
10	60.7	55.5	-9	0.380	0.376	-1
11	88.6	78.0	-12	0.360	0.360	0
12	78.3	76.0	-3	0.360	0.362	1
13	66.8	64.7	-3	0.380	0.371	-2
14	90.0	86.7	-4	0.360	0.348	-3
15	87.7	83.7	-5	0.361	0.351	-3

As can be seen in Table 4.3, the deviations are between -13 and 5% for CO_2 removal and between -3 and 5% for the rich loading. Rich loading deviations are considerably lower than

that for CO_2 removal; therefore, it is possible to conclude that the rich loading is less sensible to errors, being the CO_2 removal a better measure of the model accuracy.

It can also be noticed that CO_2 capture tends to be under-calculated. Nevertheless, a maximum deviation of 13% is deemed acceptable considering that this is a predictive model.

Furthermore, the mean squared error of prediction (MSEP in equation 4.4) has a value of 0.003 for CO_2 removal and 0.00006 for the rich loading.

$$MSEP = \frac{\sum_{i=1}^{N_{runs}} \left(v_i^{sim} - v_i^{exp}\right)^2}{N_{runs}} \tag{4.4}$$

The relation between the values of CO_2 removal obtained through simulation and the experimental ones is shown in Figure 4.2.

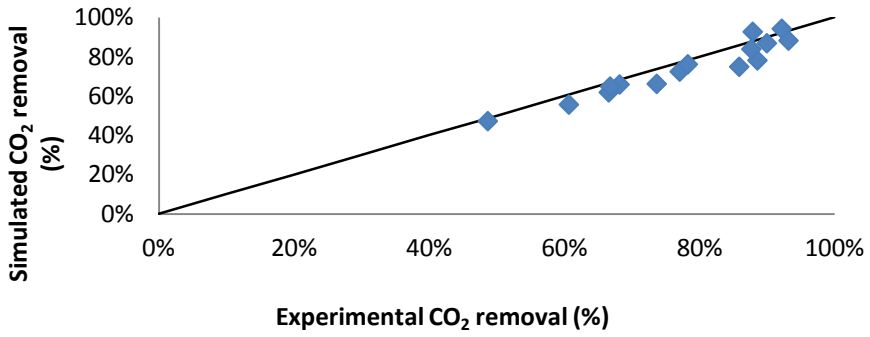

Figure 4.2 - Parity diagram of the CO_2 removal.

Besides the deviations due to the mass transfer coefficients calculation method, it should also be considered the uncertainty associated with the experimental measurements and the composition of the flue gas, for which the only information given is the CO_2 content and was thus assumed to be water saturated.

Both liquid and vapour phase temperature profiles obtained through simulation for run 1 are represented in Figure 4.3.

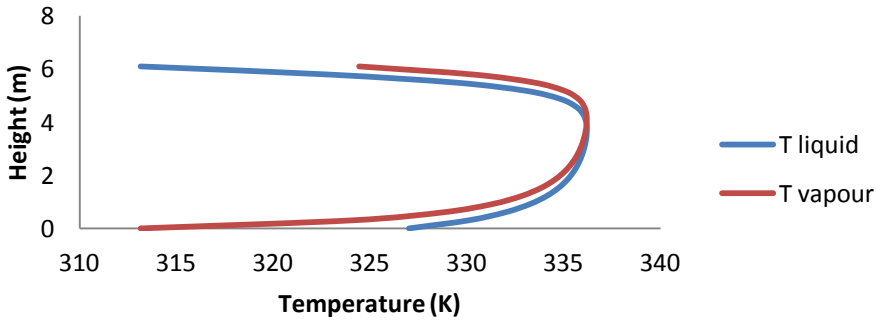

Figure 4.3 - Liquid and vapour phase temperature profiles for Run 1.

Due to the highly exothermic nature of the reaction, a lot of heat is released. The liquid takes up this heat and, since it has low specific heat, its temperature rises. The absorber exhibits a temperature bulge at the top of the column since the reaction velocity is high where the lean solvent enters.

4.2. Intercooled absorber model validation

In the same pilot plant campaign, intercooling (IC) was retrofitted to the existing absorber and two new experiments were conducted, being the available conditions and results presented in Table 4.4.

Table 4.4 - Pilot plant conditions and results using an absorber with intercooling.

Run	PZ concentration (m)	L/G (mol L/ mol G)	Loading (mol CO_2/ mol alk)		Removal (%)
			Lean	Rich	
1	7.5	4.5	0.290	–	80.0
2	8	5.9	0.294	0.374	90.0

The validation of the model built in gPROMS® that is shown in Figure 4.4 was also achieved through the comparison of the CO_2 removal and the rich loading between the experimental available values and simulated results.

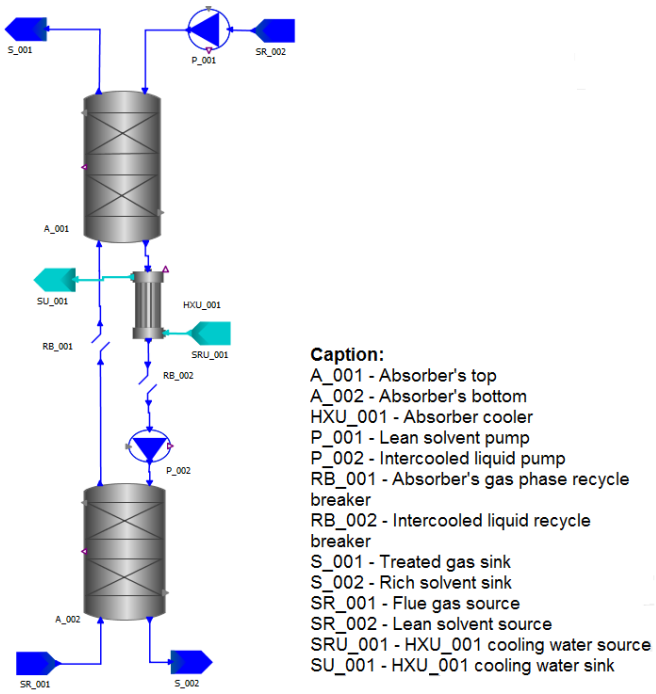

Figure 4.4 - Intercooled absorber model used for validation.

Table 4.5 shows the experimental data and simulation results for the intercooled absorber, along with the deviation between them.

Table 4.5 - Experimental and simulation results for CO_2 removal and rich loading with an intercooled absorber.

Run	CO_2 removal (%)			Rich loading (mol_{CO2}/mol_{alk})		
	Experimental	Simulation	Deviation (%)	Experimental	Simulation	Deviation (%)
1	80	79	-2	-	0.383	-
2	90	96	6	0.374	0.376	0

4.3. Stripper modelling

The only information given regarding the stripping process occurring in the pilot plant campaigns is its pressure, being this 1.38 kPa. Therefore, the starting point for the modelling of the CO_2 capture plant was the pressure given and a reboiler temperature of 380 K, which is the one usually used on MEA's capture plants.

The model assembled that is presented in Figure 4.5 is difficult to initialise since it contains two close loops. First of all the stripper alone has to be initialised alone using the procedure described in section 3.3. After this, reboiler and condenser are added to the flowsheet leaving two open loops, i.e. using sinks and sources instead of the recycle breakers RB_001 and RB_002.

Then the inputs of the stripper are changed gradually, one at the time, until the outlet conditions verified on the condenser and reboiler are equal to the inputs on the stripper. At that moment it is possible to close the loop with the help of recycle breakers.

Stripper pressure is defined through reboiler's pump (P_003).

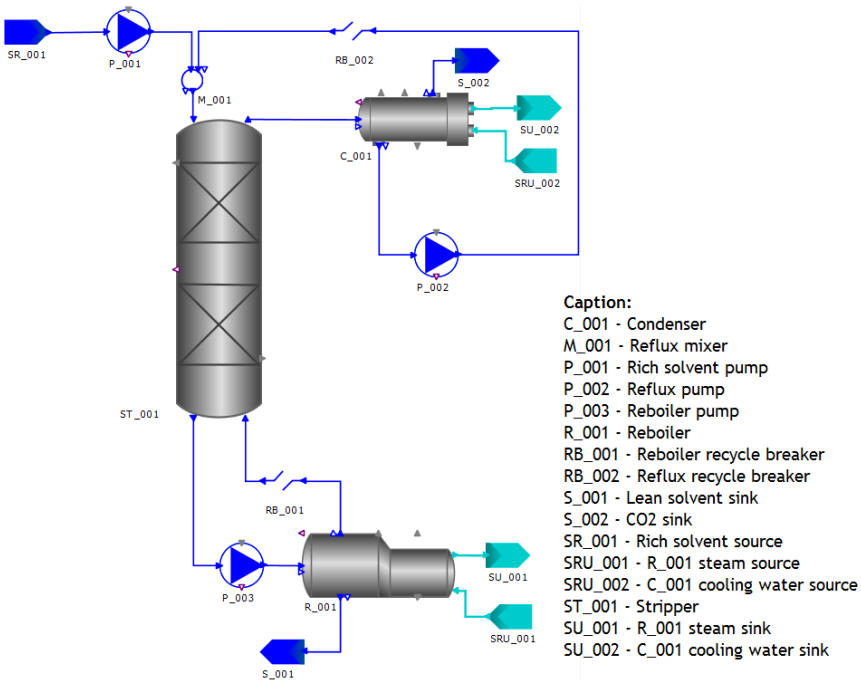

Figure 4.5 - Stripper model used for validation.

5 Piperazine Capture Plant Models

5.1. Process configurations for CO_2 capture

Five models were assembled on gPROMS® to evaluate the effects of different process configurations on heat duty and on CO_2 capture evaluation parameters.

In order to be possible to compare them, lean solvent and flue-gas streams were kept constant, as well as the utilities used for heat exchange: cooling water (20 °C, 1 atm) and saturated steam (151 °C, 5 bar). Rich solvent temperature is set to be 370 K and stripper pressure is kept at 1.38 bar for all the configurations that include this equipment.

Flue gas conditions are as previously presented on Table 4.2. Solvent make-up is defined to keep a lean solvent mass flowrate of 1.00 kg/s and a PZ mass fraction of 0.364.

5.1.1 Case A: Simple absorber and simple stripper configuration

A complete flowsheet consisting of a simple absorber and a simple stripper for CO_2 capture was assembled with gPROMS® (see Figure 5.1) based on the available data from the November 2008 campaign.

Absorber and stripper models have the same configuration as the ones that were presented and validated in the previous section. Pump models P_001, P_002 and P_005 are required without any specification before the stripper, absorber and heat exchanger inlet, respectively, to provide the required pressure for the liquid phase in each model. P_003 outlet pressure is 1.38 bar, which corresponds to the stripper and reboiler pressure. P_004 outlet pressure is set to 1.21 bar so that, considering all the pressure drops, the inlet pressure at the absorber is 1.01 bar.

In the heat exchanger HXU_001, the process stream is cooled using cooling water down to 313.15 K, which corresponds to the inlet temperature in the absorber. Heat exchanger HX_001 input is the cold stream outlet temperature and it was set to 370 K.

Condenser temperature was set to 310 K and reboiler's to 380 K. These temperatures are achieved using a certain amount of utility, which is calculated by the program.

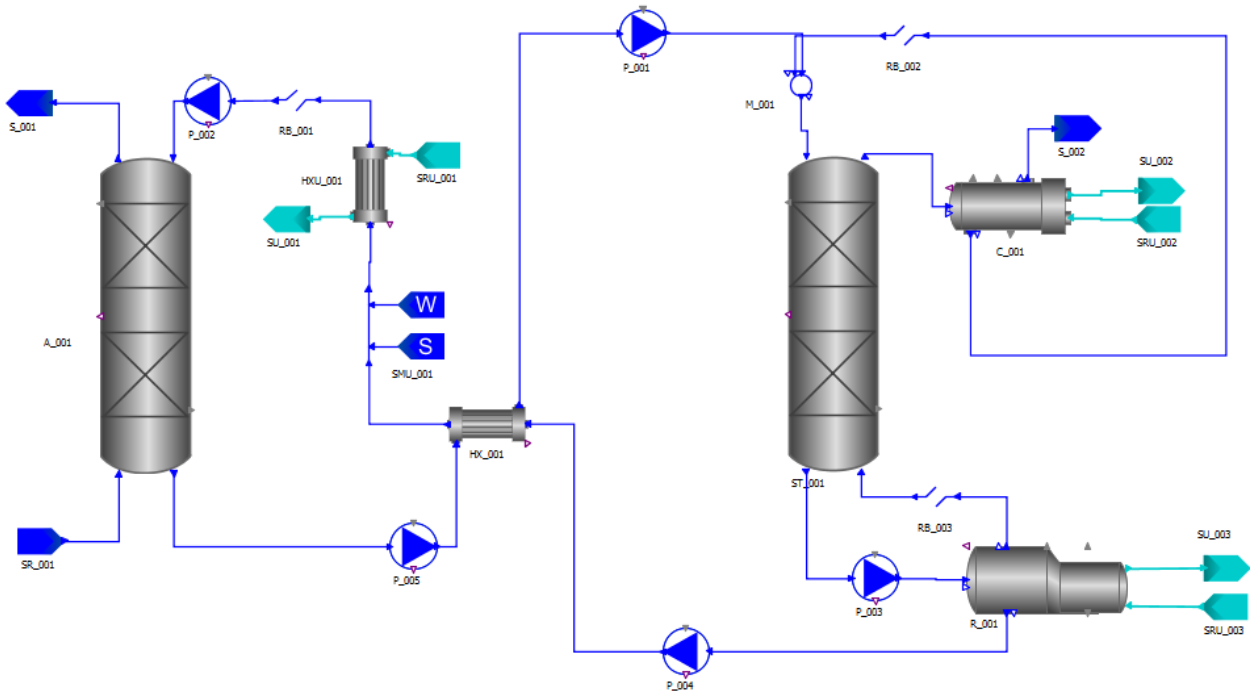

Caption:

A_001	Absorber	P_005	Rich solvent pump (before HX_001)	SR_001	Flue gas source
C_001	Condenser	R_001	Reboiler	SRU_001	HXU_001 cooling water source
HX_001	Lean-rich heat exchanger	RB_001	Absorber recycle breaker	SRU_002	C_001 cooling water source
HXU_001	Lean solvent cooler	RB_002	Reflux recycle breaker	SRU_003	R_001 steam source
M_001	Reflux mixer	RB_003	Reboiler recycle breaker	ST_001	Stripper
P_001	Rich solvent pump (after HX_001)	S_001	Treated gas sink	SU_001	HXU_001 cooling water sink
P_002	Lean solvent pump (after HX_001)	S_002	CO_2 sink	SU_002	C_001 cooling water sink
P_003	Reboiler pump	SMU_001	Solvent make-up	SU_003	R_001 steam sink
P_004	Lean solvent pump (before HX_001)				

Figure 5.1 - Flowsheet of the simple absorber and simple stripper configuration.

5.1.2 Case B: Intercooled absorber and simple stripper

After being validated, the intercooled absorber was integrated in a complete flowsheet, as can be seen in Figure 5.2. This configuration is equal to the one used on September and December 2010 pilot plant campaigns.

Intercooled absorber and stripper models are equal to the ones that were validated in the previous section. Pump models P_003, P_004, P_005 and P_006 are required without any specification before the heat exchanger, stripper, absorber and intercooling, respectively, for the same reason of Case A. P_001 outlet pressure is also 1.38 bar, which corresponds to the stripper and reboiler pressure. P_002 outlet pressure is set to 1.21 bar so that, considering all the pressure drops, the inlet pressure at the absorber is 1.01 bar.

In the heat exchanger HXU_001 the liquid stream from the middle of the absorber is cooled down to 313.15 K, which corresponds to the intercooling temperature. Heat exchanger HXU_002 is also set to 313.15 K, which is the inlet temperature in the absorber. The required inputs for HX_001 for the condenser and the reboiler are the same as for Case A.

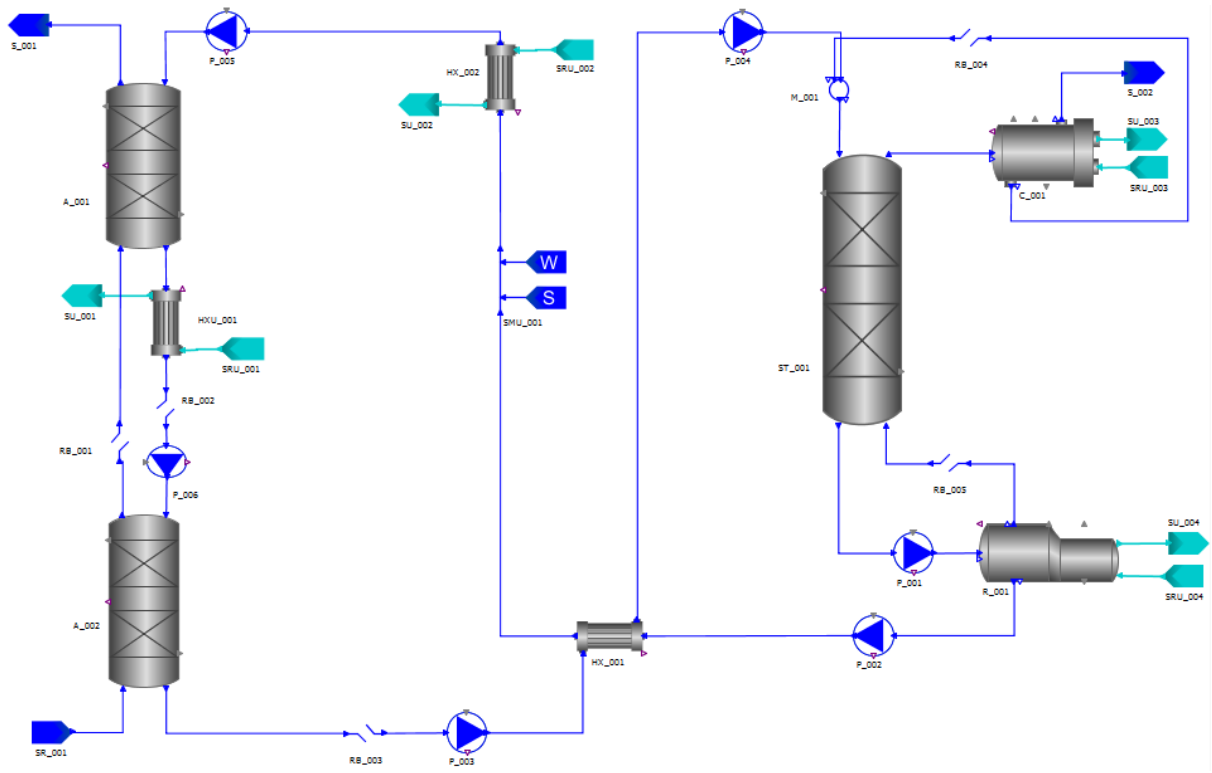

Caption

A_001	Absorber's top	P_005	Lean solvent pump (after HX_001)	SR_001	Flue gas source
A_002	Absorber's bottom	P_006	Intercooling pump	SRU_001	HXU_001 cooling water source
C_001	Condenser	R_001	Reboiler	SRU_002	HXU_002 cooling water source
HX_001	Lean-rich heat exchanger	RB_001	Absorber's gas phase recycle breaker	SRU_003	C_001 cooling water source
HXU_001	Absorber cooler	RB_002	Intercooled liquid recycle breaker	SRU_004	R_001 steam source
HXU_002	Lean solvent cooler	RB_003	Rich solvent recycle breaker	ST_001	Stripper
M_001	Reflux mixer	RB_004	Reflux recycle breaker	SU_001	HXU_001 cooling water sink
P_001	Reboiler pump	RB_005	Reboiler recycle breaker	SU_002	HXU_002 cooling water sink
P_002	Lean solvent pump (before HX_001)	S_001	Treated gas sink	SU_003	C_001 cooling water sink
P_003	Rich solvent pump (before HX_001)	S_002	CO_2 sink	SU_004	R_001 steam sink
P_004	Rich solvent pump (after HX_001)	SMU_001	Solvent make-up		

Figure 5.2 - Flowsheet of the intercooled absorber and simple stripper configuration.

5.1.3 Case C: Simple absorber and stripper with lean vapour recompression

A flash-drum at atmospheric pressure was added to the simple absorber and simple stripper system, as shown in Figure 5.3.

Absorber and stripper models are equal to the ones that were validated in the previous section. Pump models P_001, P_002 and P_003 are required without any specification before the stripper, absorber and heat exchanger, respectively, as explained for Case A. P_004 outlet pressure is also 1.38 bar, which corresponds to the stripper and reboiler pressure. P_005 outlet pressure is set to 1.11 bar and corresponds to the flash pressure. P_003 represents the compressor utilized to increase the lean vapour pressure back to 1.38 bar.

Heat exchangers HXU_001 and HX_001, reboiler and condenser input specifications are the same as for the previous case.

The flash model requires the specification of the initial phase and the temperature initial guess, which in this case are two-phase and 380 K, respectively.

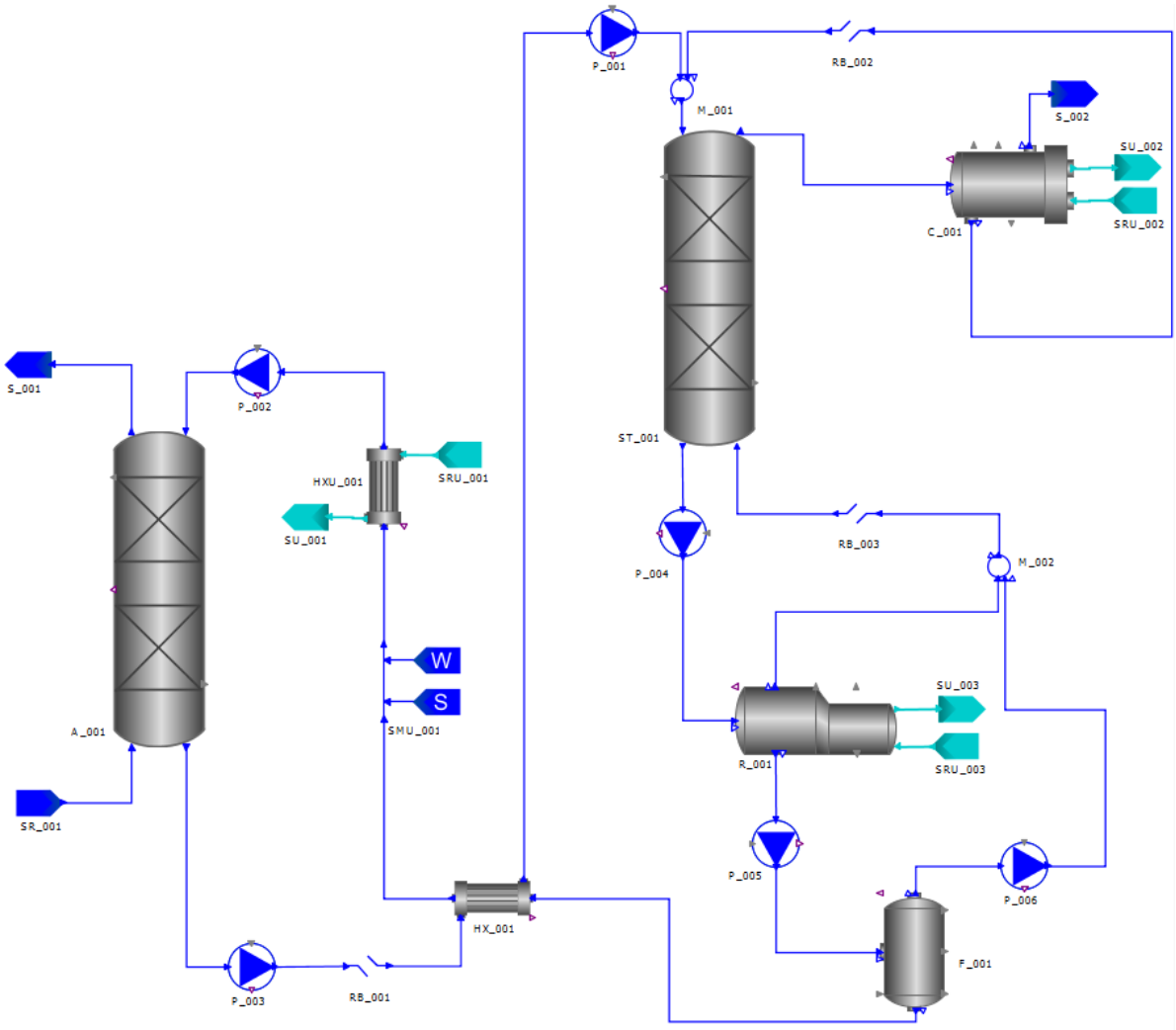

Caption:

A_001	Absorber	P_004	Reboiler pump	SMU_001	Solvent make-up
C_001	Condenser	P_005	Flash pump	SR_001	Flue gas source
F_001	Flash	P_006	Lean vapour compressor	SRU_001	HXU_001 cooling water source
HX_001	Lean-rich heat exchanger	R_001	Reboiler	SRU_002	C_001 cooling water source
HXU_001	Lean solvent cooler	RB_001	Rich solvent recycle breaker	SRU_003	R_001 steam source
M_001	Reflux mixer	RB_002	Reflux recycle breaker	ST_001	Stripper
M_002	Reboiler and flash mixer	RB_003	Reboiler recycle breaker	SU_001	HXU_001 cooling water sink
P_001	Rich solvent pump (after HX_001)	S_001	Treated gas sink	SU_002	C_001 cooling water sink
P_002	Lean solvent pump (after HX_001)	S_002	CO_2 sink	SU_003	R_001 steam sink
P_003	Rich solvent pump (before HX_001)				

Figure 5.3 - Flowsheet of the simple absorber and stripper with lean vapour recompression configuration.

With this configuration, the hot lean solvent leaving the stripper column is vaporized in a flash drum at low pressure, and the vapours released by this process are compressed and reinjected, supplying the additional steam enthalpy directly at the stripper bottom, thus reducing energetic needs of the reboiler.

However, this process modification entails additional energy requirements to compress the flashed vapours that will not be considered in this study. Nevertheless, according to Reddy

et al., 2007, even considering the increase in electrical power, the net energy requirement of the system is decreased.

5.1.4 Case D: Intercooled absorber and stripper with lean solvent recompression

The flash drum was also integrated in the intercooled absorber and simple stripper system, being the model built shown in Figure 5.5.

Absorption section specifications are the same as for Case B and stripping specifications are the same as for Case C.

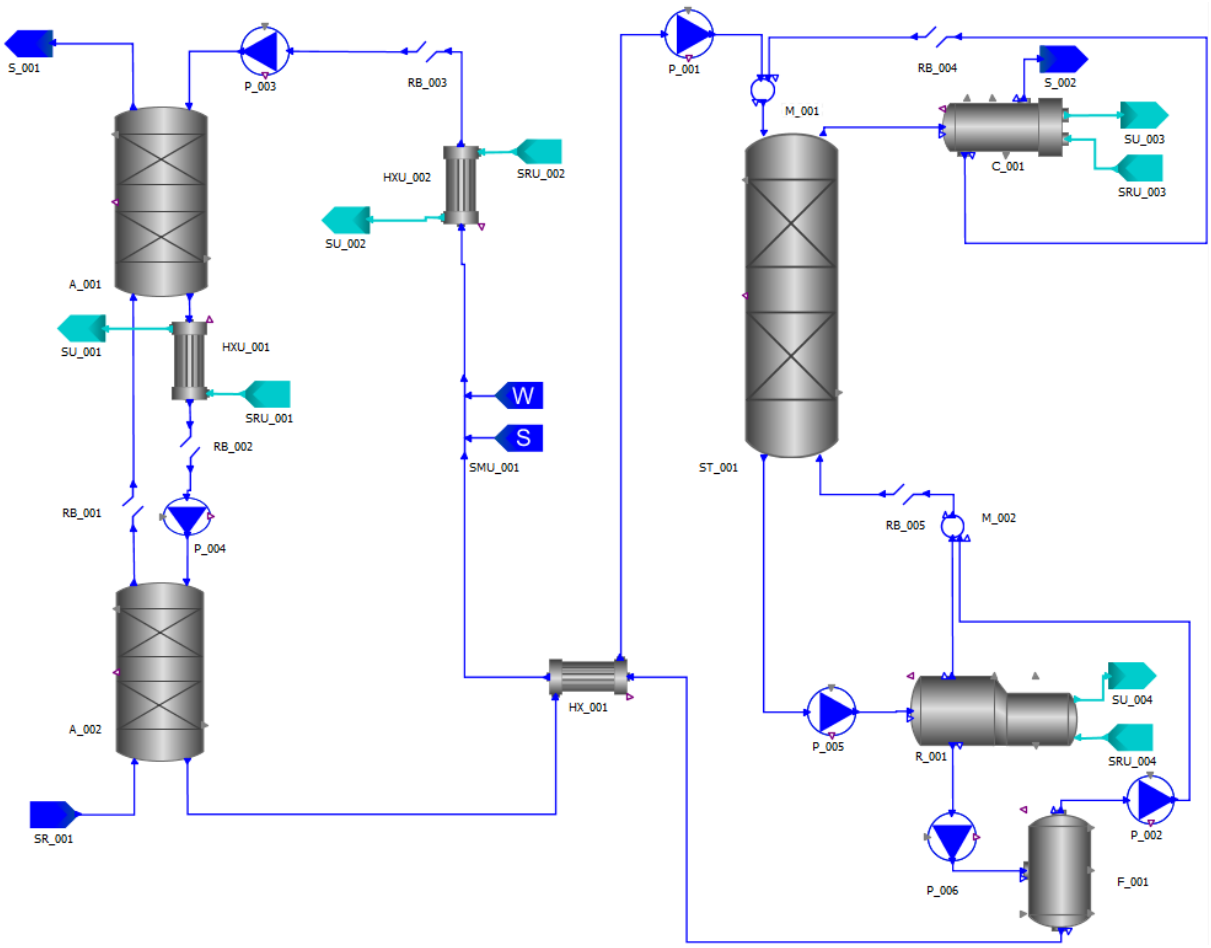

Caption:

A_001	Absorber's top	P_004	Intercooling pump	SMU_001	Solvent make-up
A_002	Absorber's bottom	P_005	Reboiler pump	SR_001	Flue gas source
C_001	Condenser	P_006	Flash pump	SRU_001	HXU_001 cooling water source
F_001	Flash	R_001	Reboiler	SRU_002	HXU_002 cooling water source
HX_001	Lean-rich heat exchanger	RB_001	Absorber's gas phase recycle breaker	SRU_003	C_001 cooling water source
HXU_001	Absorber cooler	RB_002	Intercooled liquid recycle breaker	SRU_004	R_001 steam source
HXU_002	Lean solvent cooler	RB_003	Lean solvent recycle breaker	ST_001	Stripper
M_001	Reflux mixer	RB_004	Reflux recycle breaker	SU_001	HXU_001 cooling water sink
M_002	Reboiler and flash mixer	RB_005	Reboiler recycle breaker	SU_002	HXU_002 cooling water sink
P_001	Rich solvent pump (after HX_001)	S_001	Treated gas sink	SU_003	C_001 cooling water sink
P_002	Condensate pump	S_002	CO_2 sink	SU_004	R_001 steam sink
P_003	Lean solvent pump (after HX_001)				

Figure 5.4 - Flowsheet of the intercooled absorber and stripper with integrated flash configuration.

5.1.5 Case E: Intercooled absorber and two flashes

A new configuration based on the October 2011 Pilot Plant campaign conducted at the University of Texas was assembled with gPROMS®, as shown in Figure 5.6.

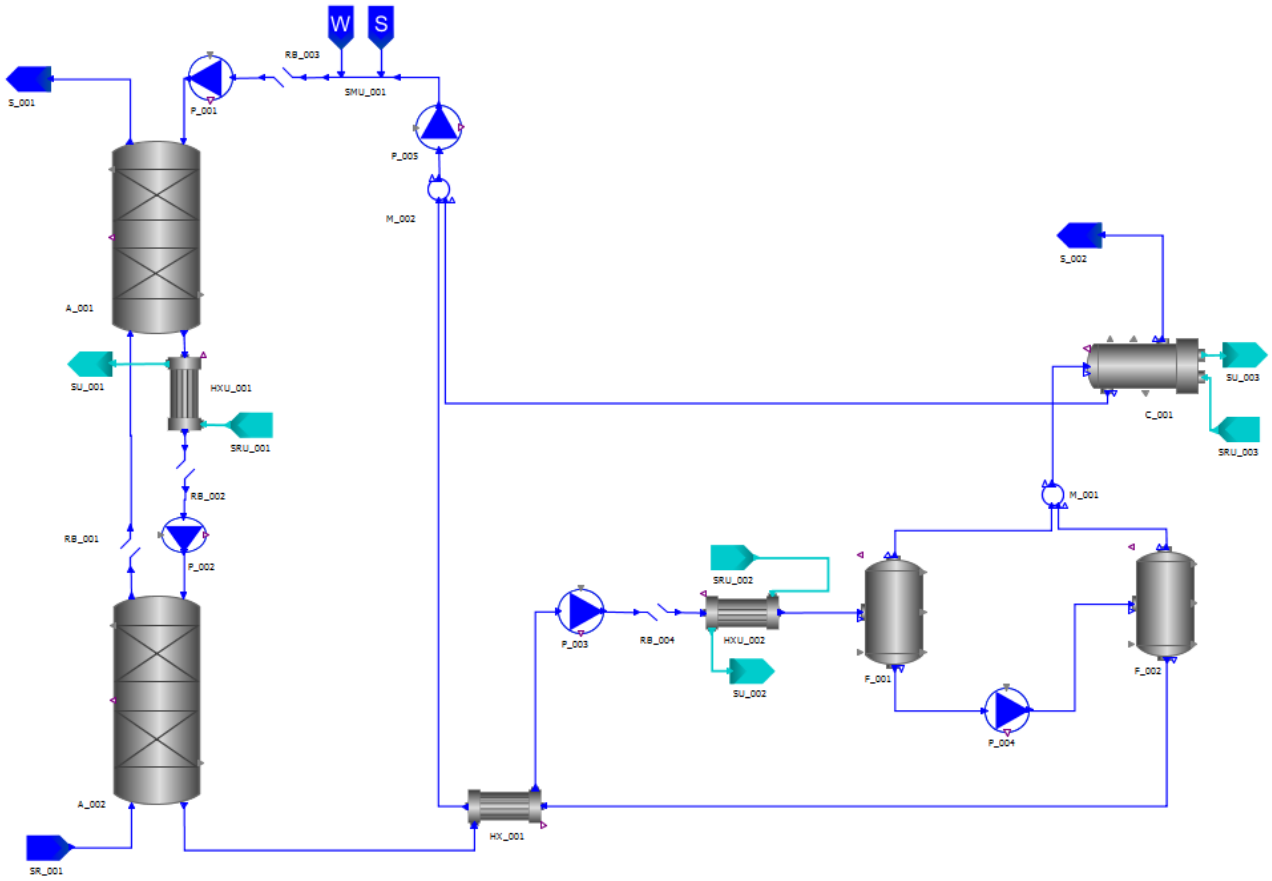

Caption:

A_001	Absorber's top	P_001	Absorber's inlet pump	S_002	CO_2 sink
A_002	Absorber's bottom	P_002	Intercooling pump	SMU_001	Solvent make-up
C_001	Condenser	P_003	High-pressure flash pump	SR_001	Flue gas source
F_001	High-pressure Flash	P_004	Low-pressure flash pump	SRU_001	HXU_001 cooling water source
F_002	Low-pressure Flash	P_005	Lean solvent pump	SRU_002	HXU_002 steam source
HX_001	Lean-rich heat exchanger	RB_001	Absorber's gas phase recycle breaker	SRU_003	C_001 cooling water source
HXU_001	Absorber cooler	RB_002	Intercooled liquid recycle breaker	SU_001	HXU_001 cooling water sink
HXU_002	Rich solvent heater	RB_003	Lean solvent recycle breaker	SU_002	HXU_002 steam sink
M_001	Vapour mixer	RB_004	Flash inlet recycle breaker	SU_003	C_001 cooling water sink
M_002	Condensate and rich solvent mixer	S_001	Treated gas sink		

Figure 5.5 - Flowsheet of the intercooled absorber and two flash configuration.

Pump models P_001 and P_002 are required without any specification before the absorber and in the intercooling, respectively, as explained for Case A. P_003 outlet pressure is 10 bar and corresponds to the high pressure (HP) flash. P_004 is the valve used to decrease the pressure inlet in the low pressure (LP) flash, and is set to the value of 5.5 bar. P_005 outlet pressure is set to 1.11 bar so the inlet pressure at the absorber can be 1.01 bar.

HP and LP flash pressures used in this simulation are based on pilot data provided by Walters et al. 2013.

HXU_001 is the heat exchanger used to cool the liquid phase at the middle of the column until 313.15 K. In the heat exchanger HX_001 the cold stream coming from the absorber is heated to 405 K by the rich solvent coming from the desorption section. An additional heat exchanger, HXU_002, uses steam as utility to heat the lean solvent until 423.15 K, which corresponds to the flash section temperature.

Both flashes and the condenser require the specification of a temperature initial guess, being that 423.15 and 310 K, respectively.

Since this configuration does not have a reboiler, the energy needed is provided by steam in heat exchanger HXU_002.

5.2. Process configurations comparison

The results obtained through simulation for each configuration are presented on Table 5.1.

Table 5.1 - Performance results for every configuration analysed.

Case	Loading (mol CO_2/mol alk)		CO_2 capture (%)	Deviation (%)	PZ losses (kg/s)	CO_2 stripped (kg/s)	Heat duty (kJ/kg CO_2)	Deviation (%)
	Lean	Rich						
A	0.266	0.347	88.2	-	3.46×10^{-5}	0.0295	5229	-
B	0.267	0.356	98.6	+12	3.94×10^{-5}	0.0330	4924	-6
C	0.261	0.343	90.8	+3	3.55×10^{-5}	0.0304	4517	-14
D	0.261	0.350	98.9	+12	3.88×10^{-5}	0.0330	4382	-16
E	0.314	0.372	63.2	−28	1.57×10^{-3}	0.0212	4372	-16

For case A, which corresponds to the conventional configuration, the solvent stream fed to the absorber has a CO_2 loading of 0.266 mol/mol, and the rich solvent leaving the column has a loading of 0.347 mol/mol. 88.2 % of the carbon dioxide is captured in the absorber and sent to the stripper. In the desorption column, 0.0295 kg/s of CO_2 are stripped and 3.46×10^{-5} kg/s of PZ are lost in both gaseous streams.

The heat duty associated to this process configuration is 5229 kJ/kg CO_2 stripped, and corresponds entirely to the energy input needed at the reboiler. Heat duty calculations are presented in Appendix 4. Deviations presented in Table 5.1 are calculated relatively to this configuration.

Configuration B differs from the previous one in that it has intercooling placed at the middle of the absorber column, which can significantly improve process performance by increasing

solvent capacity. CO_2 capture is increased by $12\ \%$ and heat duty has decreased 305 kJ/kg CO_2.

The inclusion of the flash model in the conventional configuration assembled in case C had the expected effect on heat duty. Energetic needs were reduced by $14\ \%$, while the CO_2 capture was slightly improved. However, this configuration entails a significant increase in the electricity consumption and equipment costs that are not being considered in this study. P_006 model represents a compressor responsible for raising the pressure from near atmospheric P to 1.38 bar, which requires significantly more energy than any of the existing pumps (Reddy et al., 2008).

The flash model was also added to the intercooled absorber and simple stripper configuration, which resulted on configuration D. CO_2 capture did not change notably relatively to configuration B, which corresponds to this configuration without the lean vapour compression, but a significant improvement was observed on the heat duty of the reboiler.

Configuration E is different from all the previous since it uses two sequential flashes instead of the stripper for CO_2 desorption. For the conditions studied, CO_2 capture is only $63.2\ \%$, $28\ \%$ lower than that for the conventional process. However, this process reduces by $16\ \%$ the energy requirements per amount of CO_2 stripped. Besides low carbon capture, this process configuration has significantly higher solvent losses, when compared to the previous one presented. To improve these parameters more flash models could be added to the process, thus improving CO_2 desorption.

A detailed description of the inputs and simulation results for every configuration is presented in Appendix 5.

6 Sensitivity analysis and Optimisation

6.1 Sensitivity analysis

A sensitivity analysis was carried out with regard to several variables comprised in the capture plant models, in order to understand their effect on the heat duty and on CO_2 capture parameters.

6.1.1 Intercooling effect on absorber's performance

As mentioned in section 4.2, intercooling was placed in the middle of the absorber column and its temperature was set to reach a value of 40 ºC, so the model could reproduce the experiments conducted at the University of Texas and thus be validated.

Under the assumption that the validation results presented in the Models Validation section are still valid for different conditions and absorber configurations, some alterations were made in order to analyse the effect of intercooling temperature and position.

6.1.1.1 Intercooling temperature effect

The first analysis aims to identify the intercooling temperature effect on CO_2 capture and rich loading. To accomplish this, the difference between inlet and outlet process temperatures in the Heat-Exchanger was varied from zero to its upper limit, using the gPROMS® model presented in Figure 4.4.

The situation of $\Delta T = 0$ corresponds to the simple absorber case, i.e., without intercooling. The upper limit is set by the minimum temperature difference in the Heat-Exchanger of 5 ºC between the process and utility streams, considering that the last one is cooling water at 20 ºC.

Using the data from Run 1 that is presented in Table 4.5 as input to a simple absorber, a CO_2 capture of 64 % can be achieved. When decreasing the temperature of the middle column intercooling while keeping the lean solvent and flue gas input constants, a proportional increase is verified in the CO_2 capture rate, as can be seen in Figure 6.1.

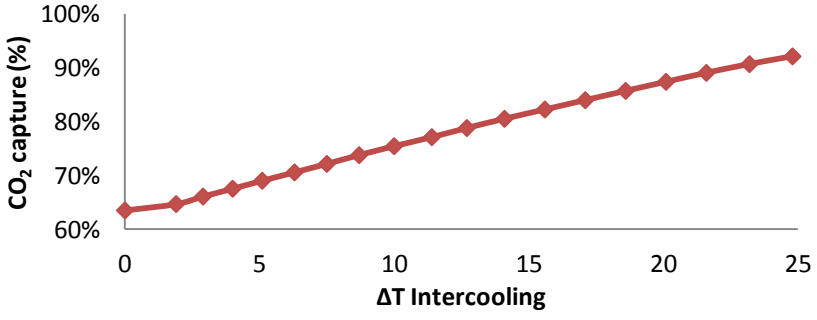

Figure 6.1 - Intercooling temperature effect.

The intercooled absorber set to the maximum decrease of temperature presents a CO_2 capture of $92\ \%$, which represents an increase of $44\ \%$ relatively to the simple absorber. The effects on the rich loading are not as significant, showing an increase of 9%, for this case.

Relatively to the pilot plant case, where the intercooling temperature was $40\ ^{o}C$, it is possible to increase CO_2 capture rate by $17\ \%$ when using the lower intercooling temperature allowed (298.15 K). However, this would represent an increase of $82\ \%$ of the utility mass flowrate. An in depth analysis should be made in order to verify whether it would be economically advantageous to use lower intercooling temperatures for this CO_2 capture configuration.

This analysis demonstrates that CO_2 capture can be enhanced by integrating intercooling within the absorption column. According to Jung et al., 2015 and Frailie et al., 2013, intercooling can provide thermodynamically driven mass transfer in the lower stages of the absorber by maintaining a higher loading of CO_2 in the solvent, which can increase the solvent's absorption capacity.

According to Cousins et al., 2015, the benefits of intercooling depend on the operating conditions of the plant: higher L/G ratios can present more pronounced effect.

6.1.1.2 Intercooling position effect

A further analysis was made to verify if the intercooling position affects the results obtained. Table 6.1 shows simulation results for three intercooling positions: middle top ($Z/Z_T = 1/3$), middle ($Z/Z_T = 1/2$) and middle bottom ($Z/Z_T = 2/3$) for three intercooling temperatures.

Rich loading results are not affected by the intercooling position.

Table 6.1 - Intercooling position effect at different temperatures.

T_{IC} (K)	320		313		298	
Z/Z_T	CO_2 *capt.* (%)	Deviation (%)	CO_2 *capt.* (%)	Deviation (%)	CO_2 *capt.* (%)	Deviation (%)
1/3	72.7	-1.44	78.5	-1.46	91.1	-1.07
1/2	73.8	-	79.7	-	92.1	-
2/3	73.8	-0.03	79.7	0.02	92.2	0.08

Deviations shown in Table 6.1 are calculated relatively to middle column intercooling results, which is the configuration that has been validated with experimental data. Middle top intercooling presents slightly lower CO_2 capture rates and middle bottom results are similar to the ones for middle column intercooling.

CO_2 absorption is an exothermic process and the heat produced leads to an increase in the temperature of the solvent, which will limit the driving force for absorption and hence lower

the absorption capacity of the solvent system. Thermodynamically, CO_2 absorption reactions are favoured by lower temperature, whilst reaction kinetics, viscosities and diffusion coefficients are more favourable at higher temperature. Since the absorber model is operated adiabatically, these two effects will be competing with each other (Cousins, Wardhaugh, and Feron 2011).

As can be seen in Figure 6.2, there are two different zones in the absorber column: the rate limited section and the equilibrium limited one. The first one is located at the top of the column and presents the higher CO_2 capture rate. In this zone the temperature is high, which disfavours CO_2 loading but increases reaction rate; moreover it is near lean loading input, meaning that the loading driving force is high enough to counterbalance the effects of high temperature on it.

The equilibrium limited section comprises the middle and middle bottom region of the column, where CO_2 capture has minor alterations. In this zone, operational line is closer to the equilibrium one and thus the driving force is smaller, which leads to smaller capture rates.

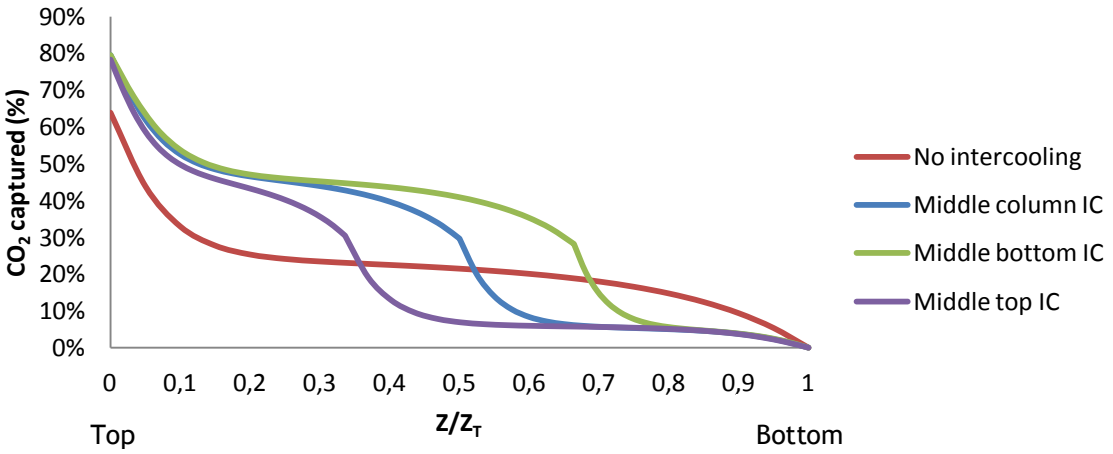

Figure 6.2 - Intercooling position effect on CO_2 capture profile ($T_{IC} = 313.15\ K$).

There is no advantage in placing intercooling at the top, since it is a rate based zone, enhanced by higher temperatures and the driving force is already high enough, as can be seen in Figure 6.3.

When decreasing temperature in the equilibrium limited section, there is a momentary increase of the driving force, which is the difference between equilibrium and operating lines, leading to an increase in the capture rate at the same point, as shown in Figure 6.2 and Table 6.2.

As can be seen in Figure 6.3, intercooling improves solvent capacity.

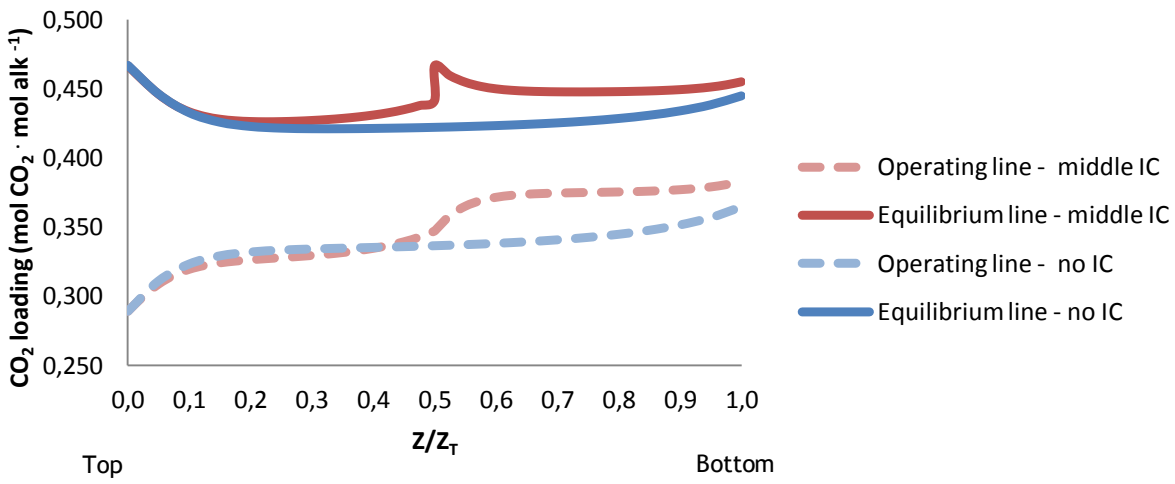

Figure 6.3 - Operating and equilibrium lines with and without intercooling.

Equilibrium line determination process and the values presented on Table 6.2 for the other intercooling locations are presented in Appendix 6.

Table 6.2 - Operating, equilibrium and driving force values for CO_2 loading with intercooling at middle.

Z/Z_T	T_{liq} (K)	CO_2 loading (mol CO_2/mol alk)		Driving force
		operating	equilibrium	
0.00	313.15	0.289	0.467	0.177
0.05	324.38	0.309	0.446	0.137
0.10	330.14	0.319	0.433	0.114
0.15	332.36	0.324	0.428	0.104
0.20	333.04	0.326	0.426	0.100
0.30	332.73	0.329	0.427	0.098
0.40	331.11	0.335	0.431	0.096
0.50	**313.15**	**0.347**	**0.467**	**0.120**
0.55	320.04	0.365	0.455	0.090
0.60	322.48	0.371	0.450	0.079
0.65	323.30	0.374	0.448	0.075
0.70	323.54	0.374	0.448	0.073
0.80	323.47	0.375	0.448	0.073
0.90	322.77	0.377	0.449	0.072
1.00	319.86	0.383	0.455	0.072

Temperature profiles for different intercooling positions are shown in Figure 6.4.

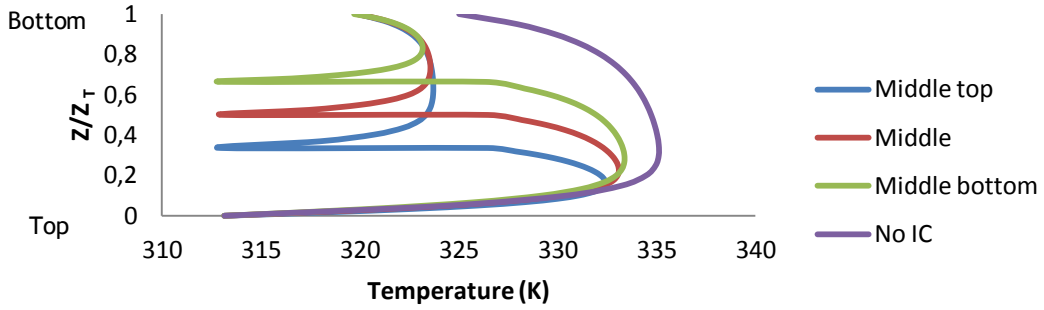

Figure 6.4 - Temperature profiles for intercooling at T=313.15 K.

Both intercooling temperature and position analyses results would have been different if other parameters were changed. According to Walters et al., 2013 the intercooling effect is more pronounced at higher solvent flowrate due to the higher sensible heat, and hence higher cooling capacity, of the higher solvent flowrates.

6.1.2 Intercooling effect on a complete plant performance

As for the intercooled absorber model, intercooling effect was analysed for the complete capture plant presented in Figure 5.2.

As can be seen in Figure 6.5, for these conditions there is no advantage on cooling the stream at temperatures below 53 °C since capture rate remains unaltered from that point on.

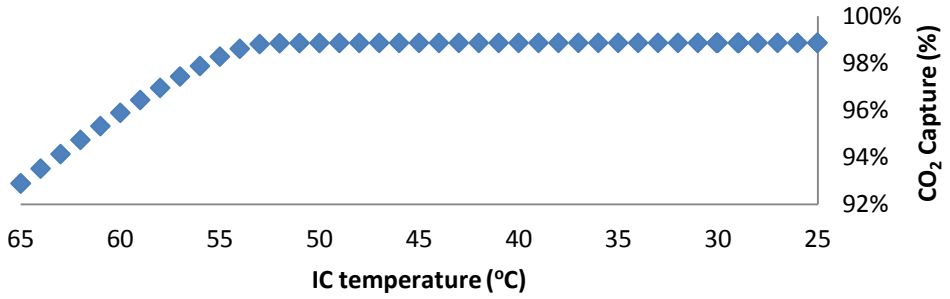

Figure 6.5 - Intercooling temperature effect on CO_2 capture.

This simulation and optimisation analysis can improve the process efficiency. For this case, with lower cooling water flowrate same results can be obtained.

However, it should be noted that these conclusions are only valid for these specific operating conditions. Each case can be easily evaluated using this model built on gPROMS®, simply running it with the desired conditions.

6.1.3 Stripper pressure effect on the conventional plant performance

Using the conventional configuration for chemical-based CO_2 capture presented in section 5.1.1, a further analysis was made in order to verify the effect of stripper pressure on the energy requirements of the reboiler. To accomplish this, CO_2 stripped variable was assigned to the value obtained with the model presented in Figure 5.1, replacing reboiler temperature as assigned variable. Therefore the assigned variables changed but the degrees of freedom of the system were kept constant.

The reboiler pressure increase is accompanied by an increase in the temperature. As the temperature increases the conditions become favourable for mass transfer of CO_2 to the gas phase and hence, less steam is required to maintain the driving force for the carbon dioxide desorption. Thus, it is favourable to operate the stripper at as high pressures and hence temperature as possible. Also, as the reboiler pressure increases, the power required for compressing the CO_2 stream for discharge conditions decrease.

The operating conditions of the reboiler are limited by solvent degradation. For PZ, a temperature higher than 150 ^{o}C is not recommended, so the stripper needs to be operated at a pressure that corresponds to a temperature of 150 ^{o}C or lower.

High desorption pressure entails higher equipment costs, which is its only disadvantage and must be considered.

Stripper pressure was varied between 1.38×10^5 and 2.5×10^5 Pa, resulting on an increase of reboiler temperature from 380.0 to 396.5 K. The increase of pressure and temperature led to a heat duty reduction of 2.2 %. Results are presented in Appendix 7.

6.1.4 L/G ratio effect on the conventional plant performance

A sensitivity analysis was made in order to understand the effect of L/G ratio on the performance of the system, also considering the conventional process configuration. Liquid flowrate was varied between 0.850 and 1.018 kg/s, which correspond to a molar flowrate of 20.85 and 25.00 mol/s, respectively. Flue gas flowrate was kept constant and equal to the one used in the other simulations.

The increase on the L/G ratio from 3.2 to 3.9 resulted on a CO_2 capture increase of 9.1 %. On the other hand, rich loading decreased 2 %. The energy requirements per amount of CO_2 stripped increased 2.1 % for higher ratios, from 4650 to 4746 kJ/kg CO_2, meaning that energy requirements are lower for lower L/G ratios.

Further results are presented in Appendix 8.

6.1.5 Piperazine concentration effect on the conventional plant performance

An analysis on the effect of piperazine concentration was also performed using the simple absorber and simple stripper configuration. To achieve this, the lean solvent PZ mass fraction defined in the solvent make-up model was varied between 0.150 and 0.375.

As can be seen in Figures 6.6 - 6.8, the increase of piperazine concentration has positive effects on heat duty and CO_2 capture but the rich loading is disadvantaged.

Piperazine concentration increase resulted on a heat duty and rich loading reduction of 15 and 10 %, respectively, and on an increase of 38 % on CO_2 capture.

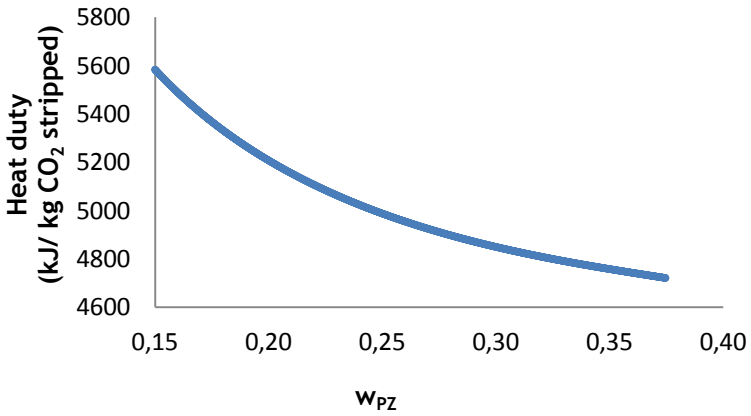

Figure 6.6 - Piperazine concentration effect on heat duty.

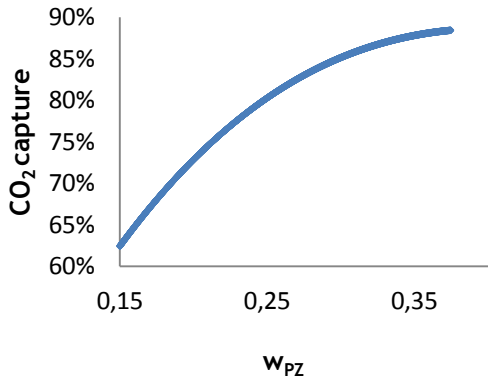

Figure 6.7 - Piperazine concentration effect on CO_2 capture.

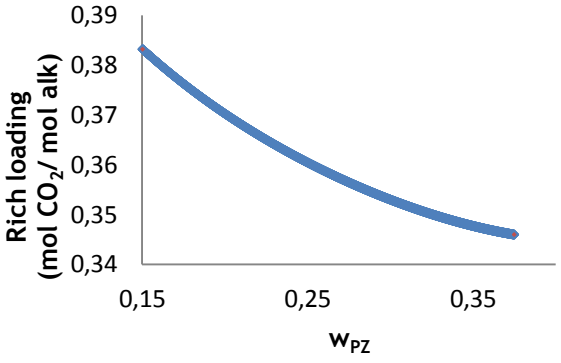

Figure 6.8 - Piperazine concentration effect on rich loading.

Piperazine concentration has an upper limit, since this solvent is known to have solubility problems encountered at both lean and rich CO_2 loadings, which leads to a limited operating range (Chen et al. 2014, Dugas and Rochelle 2011a).

The values obtained through simulation are presented in Appendix 9.

6.2 Optimisation

6.2.1 Case A

The conventional plant operating conditions were optimised using gPROMS® platform standard mathematical optimisation capabilities, so as to minimise the energy requirements at the reboiler.

Four variables were used as controls: stripper pressure (through P_003 outlet pressure), reboiler temperature, liquid flowrate and solvent concentration on the lean stream. As constrained variable this optimisation considers a CO_2 capture higher than $90\ \%$.

The results and inputs of this optimisation are presented in Table 6.3.

Table 6.3 - Optimisation inputs and results for Case A.

Variable	Optimised value	Initial value	Lower bound	Upper bound
$\boldsymbol{Stripper\ P}$ (Pa)	2.29×10^5	1.38×10^5	1.375×10^5	5×10^5
$\boldsymbol{Reboiler\ T}$ (K)	397.78	380.00	379.00	423.00
$\boldsymbol{F^{LS}}$ (kg/s)	0.5488	1.0000	0.3000	1.1000
$\boldsymbol{w_{PZ}{}^{LS}}$ (g/g)	0.400	0.364	0.360	0.400
CO_2 capture (%)	90.5	88.8	90.0	100
$\boldsymbol{H}$ (kJ/kg CO_2)	4230	5229	-	-

Before the optimisation the plant was capturing $88.8\ \%$ of the CO_2, with a heat duty of 5229 kJ/kg CO_2. Using the optimal values calculated through optimisation it is possible to increase CO_2 capture up to 90.5 % and have an energy consumption of 4230 kJ/kg CO_2, which is $19\ \%$ lower than the non-optimised one.

As can be seen in Table 6.3, the piperazine mass fraction optimized value is the upper bound previously defined. It is known that this solvent has solubility issues and cannot be used at very high concentrations. However, the limit is still being studied and has not been disclosed yet. Through these optimisation results it can be concluded that the optimal concentration corresponds to the maximum one allowed.

6.2.2 Case B

The intercooled absorber and simple stripper configuration was also optimised. Besides the control variables used for the previous case, intercooling temperature was changed in order to minimise the energy requirements.

Optimum intercooling temperature corresponds to the minimum allowed, as was previously shown on the sensitivity analysis.

As can be seen in Table 6.4, optimisation led to a decrease of 13 % on the energy requirements for this configuration. Before the optimisation the CO_2 capture was 98.6 % and after that it was reduced to 90.4 %.

90 % is an acceptable number when it comes to chemical solvent-based post-combustion CO_2 capture and most of the comparative and optimisation studies are made considering this value as the one to reach. In this case it is worth to sacrifice CO_2 capture, since it will still be high enough, to have lower energy requirements.

Table 6.4 - Optimisation inputs and results for Case B.

Variable	Optimised value	Initial value	Lower bound	Upper bound
T_{IC} (K)	298.15	313.15	298.15	314.15
***Stripper P* (Pa)**	1.52×10^5	1.38×10^5	1.375×10^5	2.5×10^5
***Reboiler T* (K)**	375.83	380.00	370.00	423.00
F^{LS} (kg/s)	0.9465	1.0000	0.3000	1.1000
$w_{PZ}{}^{LS}$ (g/g)	0.400	0.364	0.360	0.400
CO_2 capture (%)	90.4	98.6	90.0	100
H (kJ/kg CO_2)	4239	4924	-	-

6.2.3 Cases C and D

Cases C and D have improved performance since they have incorporated lean vapour recompression that can provide external energy to the system, thus reducing the heat duty in the reboiler. If these processes were optimised with the same objective function, flash pressure optimum value would be the correspondent lower bound (since for that case more vapour is produced) and stripper pressure would increase significantly, as verified for the previous optimised cases. However, the increase on the difference between these two variables would represent a significant increase on the electricity consumption in the compressor placed before the stripper.

For these cases, the objective function should be changed to comprise reboiler heat duty and compressor electricity, which can represent a large part of the total energetic consumption. Therefore, the optimisation procedure was not carried out for these configurations.

6.2.4 Case E

Unlike other configurations, Case E presented significantly worse performance regarding capture parameters. For that reason, its optimisation focused on maximizing the CO_2 capture. The optimisation results and inputs are presented in Table 6.5.

Table 6.5 - Optimisation inputs and results for Case E.

Variable	Optimised value	Initial value	Lower bound	Upper bound
T_{IC} (K)	307.27	313.15	298.15	314.15
$HP\ Flash\ P$ (Pa)	8.28×10^5	1.00×10^6	5.00×10^5	1.20×10^6
$LP\ Flash\ P$ (Pa)	4.77×10^5	5.50×10^5	2.00×10^5	1.00×10^6
F^{LS} (kg/s)	1.0423	1.0000	0.4000	1.6000
CO_2 capture (%)	76.8	63.2	-	-
H (kJ/kg CO_2)	4119	4372	-	-

As can be seen in Table 6.5, through the optimisation of both flash models pressure and liquid flowrate, it is possible to increase CO_2 capture by 22 %, until a maximum value of 76.8 %. At the same time, even though it is not being considered in the objective function, heat duty value is reduced by 6 %.

Even operating at the optimum pressures and flowrate, this process is not able to achieve the proposed CO_2 capture of 90 %. Further improvements would have to be made, such as increase the number of flash models or change the dimensions of the capture models.

Flash temperature was not considered on optimisation since it is already using the optimum and maximum allowed: 423 K. Since it was already verified that optimum PZ concentration is the higher one allowed, this variable was not considered in this optimisation procedure to keep its complexity as low as possible, thus reducing the running time.

6.2.5 Cases A and B comparison

Having the same absorber performance, it becomes easier to compare Case A and Case B results. Table 6.6 comprises the optimisation results for the conventional flowsheet (Case A) and for the intercooled absorber and simple stripper configuration (Case B). This study indicates that the inclusion of intercooling can improve energy requirements by 8 %, when all control variables presented in sections 6.2.1 and 6.2.2 are operated at their optimum conditions.

Table 6.6 - Optimised processes comparison.

Case	CO_2 capture (%)	$F_{CO2\ stripped}$ (kg/s)	Heat duty (kJ/kg CO_2)	Deviation (%)
A	90.5	0.0304	4630	-
B	90.4	0.0303	4276	-8

7 Conclusions and Future Work

7.1 Conclusions

The comparison performed between experimental and simulated results demonstrated that the correlations and assumptions added to the existent gCCS® models are capable of predicting CO_2 capture parameters accurately, for both simple and intercooled absorber. CO_2 capture rate presented a maximum deviation of -12 %, which is deemed acceptable considering that these are predictive models. Rich loading presented even lower deviations: between -3 and 5 %.

Employing piperazine as solvent, besides the conventional flowsheet, four alternative process configurations were assembled on gPROMS® in order to understand the effects of each modification made to the base case on energy requirements and CO_2 capture evaluation parameters. Inputs were kept constant to ease the comparison between models.

At the conditions analysed, the conventional flowsheet allowed a CO_2 capture of 88 %, corresponding to a heat duty of 5229 kJ/kg CO_2 stripped. The inclusion of intercooling improved significantly both CO_2 capture and heat duty, by a percentage of $+12$ and -6, respectively. The decrease of temperature provided by the intercooling allows the absorber to operate at higher loading values resulting in a reduction in stripper energy requirements.

The incorporation of lean vapour recompression in the conventional configuration resulted on an increase of 3 % on CO_2 capture and a significant decrease of 14 % on heat duty. The flash model was also added to the intercooled absorber configuration, resulting on an increase of 12 % on CO_2 capture and a reduction of 16 % on reboiler duty, compared to the first case presented. The lean vapour leaving the flash placed outside the reboiler in these two configurations can supply additional steam enthalpy directly at the stripper bottom, thus reducing energetic needs of the reboiler.

In the last configuration, the stripper was replaced by two flash models. Although the CO_2 capture obtained is significantly lower than that for the conventional configuration, its energy requirements presented reductions compared to Case A.

Being the models validated, modelling becomes a powerful and useful tool in understanding the effects of several parameters on the overall performance of the capture plant.

An analysis on intercooling temperature has shown that this variable has a significant effect on CO_2 capture. Regarding the case analysed, the sensitivity analysis has proved that is possible to increase the referred parameter by 44 %, incorporating intercooling at the lower temperature possible.

Intercooling position also has effects on CO_2 capture, although not as pronounced. Due to the existence of a rate limited section and an equilibrium one, the place where the intercooling is integrated can slightly change its performance. The results obtained through simulation confirm the theoretical assumptions found on literature that claim middle and middle bottom as the best places to integrate the intercooling.

Stripper pressure increase accompanied by an increase of temperature has shown to be capable of reducing heat duty. L/G ratio was also analysed, by changing the lean solvent recirculation flowrate. The increase of this variable resulted on an improvement of $9\,\%$ of the capture rate. Energy requirements have shown to be lower for lower L/G ratios.

PZ concentration was also varied to understand its effects on the conventional configuration performance. Its increase has shown positive effects on both heat duty and CO_2 capture.

After the sensitivity analysis, three processes were optimised using gPROMS® optimisation features. Optimisation focused on minimising the energy requirements at the reboiler for cases A and B, and on maximizing CO_2 capture for Case E. After the procedure, Case A presented an improvement of $19\,\%$ on the heat duty. Case B also presented good results compared to the non-optimal solution since the energetic needs of the reboiler decreased $13\,\%$. The optimal solution for Case E is capable of increasing CO_2 capture by $22\,\%$, consequently reducing energetic needs by $6\,\%$.

7.2 Future Work

Increasing desorption unit configuration complexity has shown to improve process performance, but in some instances the improvements may not outweigh the added capital cost. For that reason, an economical optimisation should be made, considering the minimisation of not only the energy requirements but the equipment and operating cost as well.

Amine scrubbing for CO_2 capture is a new technology that is still in development, therefore new solvents and process configurations are continuously being suggested. Other configurations can be assembled and optimised on gPROMS®, and thus further complete the comparison presented in this work. The models presented on this thesis can also be used with other solvents, in order to compare its characteristics and find the best configuration and optimal operating values for each one of them.

The optimisation processes carried out focused on the alteration of only some key operating variables that were previously studied throughout the sensitivity analysis. Other parameters could be added as controls of the optimisation, such as absorber and stripper dimensions.

8 References

Adegbulugbe, Anthony, Oyvind Christophersen, Hisashi Ishitani, William Moomaw, and Jose Moreira. 2005. IPCC Special Report on Carbon Dioxide Capture and Storage. edited by Cambridge University Press. New York.

Agency, International Energy. 2013a. CO2 Emissions from Fuel Combustion. Paris.

Agency, International Energy. 2013b. Key World Energy Statistics.

Association, Carbon Capture and Storage. "What is CCS?" Accessed May.

Billet, R., and M. Schultes. 1999. "Prediction of Mass Transfer Columns with Dumped and Arranged Packings." *Chemical Engineering Research and Design* 77 (6):498-504. doi: 10.1205/026387699526520.

Bishnoi, Sanjay, and Gary T. Rochelle. 2000. "Absorption of carbon dioxide into aqueous piperazine: reaction kinetics mass transfer and solubility." *Chemical Engineering Science* 55:5531-5543.

Boot-Handford, M. E., J.C. Abanades, E. J. Anthony, M. J. Blunt, S. Brandani, N. Mac Dowell, J. R. Fernandez, M. C. Ferrari, R. Gross, J. P. Hallett, R. S. Haszeldine, P. Heptonstall, A. Lyngfelt, Z. Makuch, E. Mangano, R. T. J. Porter, M. Pourkashanian, G. T. Rochelle, N. Sahah, J. G. Yao, and P. S. Fennell. 2014. "Carbon capture and storage update." *Energy and Environmental Science* 7:130-189.

Box, The Engineering Tool. "Properties of Saturated Steam - Pressure in Bar." Accessed June 3. http://www.engineeringtoolbox.com/saturated-steam-properties-d_457.html.

Chen, Eric, Steven Fulk, Darshan Sache, YuJeng Lin, and Gary T. Rochelle. 2014. "Pilot Plant Activities with Concentrated Piperazine." *Energy Procedia* 63:1376-1391. doi: 10.1016/j.egypro.2014.11.147.

Chen, Eric, Tarun Madan, Darschan Sachde, Matthew S. Walters, Paul Nielsen, and Gary T. Rochelle. 2013. "Pilot Plant Results with Piperazine." *Energy Procedia* 37:1572-1583. doi: 10.1016/j.egypro.2013.06.033.

Closmann, Fred, Thu Nguyen, and Gary T. Rochelle. 2009. "MDEA/Piperazine as a solvent for CO2 capture." *Energy Procedia* 1 (1):1351-1357. doi: 10.1016/j.egypro.2009.01.177.

Contactor, The. 2008. Piperazine - Why It's Used and How It Works. In *Published Quarterly*: Optimized Gas Treating Inc.

Cousins, A., L. T. Wardhaugh, and P. H. M. Feron. 2011. "A survey of process flow sheet modifications for energy efficient CO2 capture from flue gases using chemical absorption." *International Journal of Greenhouse Gas Control* 5 (4):605-619. doi: 10.1016/j.ijggc.2011.01.002.

Cousins, Ashleigh, Sanger Huang, Aaron Cottrell, Paul H. M. Feron, Eric Chen, and Gary T. Rochelle. 2015. "Pilot-scale parametric evaluation of concentrated piperazine for CO2capture at an Australian coal-fired power station." *Greenhouse Gases: Science and Technology* 5 (1):7-16. doi: 10.1002/ghg.1462.

Cuéllar-Franca, Rosa M., and Adisa Azapagic. 2015. "Carbon capture, storage and utilisation technologies: A critical analysis and comparison of their life cycle environmental impacts." *Journal of CO2 Utilization* 9:82-102. doi: 10.1016/j.jcou.2014.12.001.

Derks, Peter W., Kees J. Hogendoorn, and Geert F. Versteeg. 2005. "Solubility of N2O in and Density, Viscosity, and Surface tension of Aqueous Piperazine solutions." *Journal of Chemical & Engineering Data* 50:1947-1950.

Derks, Peter W. J., Espen S. Hamborg, J. A. Hogendoorn, John P. M. Niederer, and Geert F. Versteeg. 2008. "Densities, viscosities, and liquid diffusivities in aqueous piperazine and aqueous (piperazine + N-Methyldiethanolamine) solutions." *Journal of Chemical & Engineering Data* 53:1179-1185.

Dowell, N. Mac, F. E. Pereira, F. Llovell, F. J. Blas, C. S. Adjiman, G. Jackson, and A. Galindo. 2011. "Transferable SAFT-VR Models for the Calculation of the flui phase equilibria in reactive mixtures of carbon dioxide, water, and N-alkylamines in the context of carbon capture." *Journal of Phys. Chem.* 115 (25):8155-8168.

Dubois, Lionel, and Diane Thomas. 2013. "Postcombustion CO2 Capture by Chemical Absorption: Screening of Aqueous Amine(s)-based solvents." *Energy Procedia* 37:1648-1657. doi: 10.1016/j.egypro.2013.06.040.

Dugas, Ross E., and Gary T. Rochelle. 2011a. "CO2 Absorption Rate into Concentrated Aqueous Monoethanolamine and Piperazine." *Journal of Chemical and Engineering Data* 56:2187-2195. doi: 10.1021/je101234t.

Dugas, Ross E., and Gary T. Rochelle. 2011b. "Modeling CO2 absorption into concentrated aqueous monoethanolamine and piperazine." *Chemical Engineering Science* 66 (21):5212-5218. doi: 10.1016/j.ces.2011.07.011.

Dugas, Ross, and Gary Rochelle. 2009. "Absorption and desorption rates of carbon dioxide with monoethanolamine and piperazine." *Energy Procedia* 1 (1):1163-1169. doi: 10.1016/j.egypro.2009.01.153.

EPRI. November 2005. Program on Technology Innovation: Evaluation of Amine-based Post-combustion CO2 Capture Plants.

Freeman, Stephanie. 2008. Physical properties and heat of absorption of concentrated aqueous piperazine. In *CO2 Capture by Aqueous Absorption - Summary of 2nd Quarterly Progress Reports*: University of Texas at Austin.

Freeman, Stephanie A., Ross Dugas, David H. Van Wagener, Thu Nguyen, and Gary T. Rochelle. 2010. "Carbon dioxide capture with concentrated, aqueous piperazine." *International Journal of Greenhouse Gas Control* 4 (2):119-124. doi: 10.1016/j.ijggc.2009.10.008.

Fu, Dong, Zhixin Li, and Feng Liu. 2014. "Experiments and model for the viscosity of carbonated 2-amino-2-methyl-1-propanol and piperazine aqueous solution." *The Journal of Chemical Thermodynamics* 68:20-24.

Hilliard, M D. 2008. "A predictive thermodynamic model for an aqueous blend of potassium carbonate, piperazine and monoethanolamine for carbon dioxide capture from flue gas." Doctoral dissertation, The University od Texas at Austin.

institute, Global Carbon capture and storage. "Home | Global Carbon Capture and Storage Institute." Accessed February 21.

Institute, Global CCS. "Understanding carbon capture and storage." Accessed March 12. http://www.globalccsinstitute.com/understanding-ccs.

Institute, Global CCS. "Understanding CCS Information Resources." Accessed March 5. http://www.globalccsinstitute.com/content/information-resources.

Institute, Global CCS. 2012. "CO_2 capture Technologies: Pre combustion Capture." *EPRI*.

Institute, Global CCS. January 2012a. "CO2 Capture Technologies: Oxy combustion with CO2 capture."

Institute, Global CCS. January 2012b. CO2 Capture Technologies: Post Combustion Capture (PCC).

Jung, Jaeheum, Yeong Su Jeong, Ung Lee, Youngsub Lim, and Chonghun Han. 2015. "New Configuration of the CO2Capture Process Using Aqueous Monoethanolamine for Coal-Fired Power Plants." *Industrial & Engineering Chemistry Research* 54 (15):3865-3878. doi: 10.1021/ie504784p.

Kenig, E. Y., L. Kucka, and A. Gorak. 2003. "Rigorous modelling of reactive absorption processes." *Chemical Engineering & Technology* 26 (6):677-682.

Khan, F. M., V. Krishnamoorthi, and T. Mahmud. 2011. "Modelling reactive absorption of CO_2 in packed columns for post-combustion carbon capture applications." *Chemical Engineering Research and Design* 89 (9):1600-1608.

Kim, Inna, and Hallvard F. Svendsen. 2011. "Comparative study of the heats of absorption of post-combustion CO2 absorbents." *International Journal of Greenhouse Gas Control* 5 (3):390-395. doi: 10.1016/j.ijggc.2010.05.003.

Madan, Tarun, David H. Van Wagener, Eric Chen, and Gary T. Rochelle. 2013. "Modeling pilot plant results for CO2 stripping using piperazine in two stage flash." *Energy Procedia* 37:386-399. doi: 10.1016/j.egypro.2013.05.123.

Mazari, Shaukat A., Brahim Si Ali, Badrul M. Jan, and Idris Mohamed Saeed. 2014. "Degradation study of piperazine, its blends and structural analogs for CO2 capture: A

review." *International Journal of Greenhouse Gas Control* 31:214-228. doi: 10.1016/j.ijggc.2014.10.003.

MIT, Carbon Capture & Sequestration Technologies @. 2015a. Kemper County IGCC Fact Sheet: Carbon Dioxide Capture and Storage Project.

MIT, Carbon Capture & Sequestration Technologies @. 2015b. W.A. Parish Petra Nova Fact Sheet: Carbon Dioxide Capture and Storage Project.

Moioli, Stefania, and Laura A. Pellegrini. 2015a. "Improved rate-based modeling of the process of CO_2 capture with PZ solution." *Chemical Engineering Research and Design* 93:611-620.

Moioli, Stefania, and Laura A. Pellegrini. 2015b. "Physical properties of PZ solution used as a solvent for CO2 removal." *Chemical Engineering Research and Design* 93:720-726. doi: 10.1016/j.cherd.2014.06.016.

Muhammad, Ayyaz, Mohamed I. Abdul Mutalib, Thanabalan Murugesan, and Amir Shafeeq. 2009. "Thermophysical Properties of Aqueous Piperazine and aqueous (N-Methyldiethanolamine + Piperazine) solutions at Temperatures (298.15 to 338.15) K." *Journal of Chemical & Engineering Data* 54:2317-2321.

Plaza, Jorge M., and Gary T. Rochelle. 2011. "Modeling pilot plant results for CO2 capture by aqueous piperazine." *Energy Procedia* 4:1593-1600. doi: 10.1016/j.egypro.2011.02.029.

Plaza, Jorge Mario. 2012. "Modeling of Carbon Dioxide Absorption using Aqueous Monoethanolamine, Piperazine and Promoted Potassium Carbonate " phD, University of Texas at Austin

PSE. 2014a. "New gCCS system modelling technology used for Shell Peterhead project." Accessed May. http://www.psenterprise.com/news/press_releases/140731_shell_peterhead/index.html.

PSE. 2014b. "PSE launches gCCS - world's first full-chain modelling software." Accessed May. http://www.psenterprise.com/news/press_releases/140710_gccs/index.html.

PSE. 2015a. "gPROMS ModelBuilder." Accessed June. http://www.psenterprise.com/modelbuilder.html.

PSE. 2015b. "gSAFT advanced thermodynamics." Accessed May. http://www.psenterprise.com/gsaft.html.

Rao, A. B., and E. S. Rubin. 2002. "A Technical, Economic, and Environmental Assessment of Amine-based CO_2 Capture Technology for Power Plant Greenhouse Gas Control." *Environmental Science & Technology* 36 (20):4467-4475.

Reddy, S., J. Gilmartin, and V. Francuz. 2007. Integrated compressor/stripper configurations and methods. edited by Fluor Technologies Corporation.

Rochelle, Gary, Eric Chen, Stephanie Freeman, David Van Wagener, Qing Xu, and Alexander Voice. 2011. "Aqueous piperazine as the new standard for CO2 capture technology." *Chemical Engineering Journal* 171 (3):725-733. doi: 10.1016/j.cej.2011.02.011.

Rodriguez, Javier, Artur Andrade, Adekola Lawal, N. Samsatli, Mário Calado, Alfredo Ramos, T. Lafitte, J. Fuentes, and C. C. Pantelides. 2013. "An integrated framework for the dynamic modelling of solvent-based CO2 capture processes." *Energy Procedia* 00 (000-000).

Rubin, Edward S., Hari Mantripragada, Aaron Marks, Peter Versteeg, and John Kitchin. 2012. "The outlook for improved carbon capture technology." *Progress in Energy and Combustion Science* 38:630-671.

Sachde, Darshan, Eric Chen, and Gary T. Rochelle. 2013. "Modeling Pilot Plant Performance of an Absorber with Aqueous Piperazine." *Energy Procedia* 37:1987-2001. doi: 10.1016/j.egypro.2013.06.079.

Sachde, Darshan, and Gary T. Rochelle. 2014. "Absorber Intercooling Configurations using Aqueous Piperazine for Capture from Sources with 4 to 27% CO2." *Energy Procedia* 63:1637-1656. doi: 10.1016/j.egypro.2014.11.174.

Salazar, Juan, Urmila Diwekar, Kevin Joback, Adam H. Berger, and Abhoyjit S. Bhown. 2013. "Solvent Selection for Post-Combustion CO2 Capture." *Energy Procedia* 37:257-264. doi: 10.1016/j.egypro.2013.05.110.

Samanta, Arunkumar, and S. S. Bandyopadhyay. 2007. "Kinetics and modeling of carbon dioxide absorption into aqueous solutions of piperazine." *Chemical Engineering Science* 62:7312-7319.

SaskPower. 2015. CCS performance data exceeding expectations at world-first Boundary Dam Power Station Unit #3.

Seibert, F., E. Chen, M. Perry, S. Briggs, R. Montgomery, and G. Rochelle. 2011. "UT/SRP CO2 capture pilot plant — Operating experience and procedures." *Energy Procedia* 4:1616-1623. doi: 10.1016/j.egypro.2011.02.032.

Singh, Prachi, W. P. M. Van Swaaij, and D. W. F. Brilman. 2013a. "Energy Efficient Solvents for CO2 Absorption from Flue Gas: Vapor Liquid Equilibrium and Pilot Plant Study." *Energy Procedia* 37:2021-2046. doi: 10.1016/j.egypro.2013.06.082.

Singh, Prachi, W. P. M. Van Swaaij, and D. W. F. (Wim) Brilman. 2013b. "Energy Efficient Solvents for CO2 Absorption from Flue Gas: Vapor Liquid Equilibrium and Pilot Plant Study." *Energy Procedia* 37:2021-2046.

Thee, H., Y. A. Suryaputradinata, K. A. Mumford, K. H. Smith, G. Silva, S. E. Kentish, and G. W. Stevens. 2012. "A kinetic and process modelling study of CO_2 capture with MEA-promoted potassium carbonate solutions." *Chemical Engineering Journal* 210:271-279.

Vaidya, P. D., and E. Y. Kenig. 2007. "CO_2-Alkanolamine Reaction Kinetics: A Review of Recent Studies." *Chemical Engineering & Technology* 30 (11):1467-1474.

Van Wagener, David H., and Gary T. Rochelle. 2011. "Stripper configurations for CO2 capture by aqueous monoethanolamine and piperazine." *Energy Procedia* 4:1323-1330. doi: 10.1016/j.egypro.2011.01.190.

Van Wagener, David H., Gary T. Rochelle, and Eric Chen. 2013. "Modeling of pilot stripper results for CO2 capture by aqueous piperazine." *International Journal of Greenhouse Gas Control* 12:280-287. doi: 10.1016/j.ijggc.2012.11.018.

Walters, Matthew S., Ricardo H. Dunia, Thomas F. Edgar, and Gary T. Rochelle. 2013. "Two-Stage Flash for CO2 Regeneration: Dynamic Modeling and Pilot Plant Validation." *Energy Procedia* 37:2133-2144. doi: 10.1016/j.egypro.2013.06.092.

Wang, M., A. Lawal, P. Stephenson, J. Sidders, and C. Ramshaw. 2011. "Post-Combustion CO2 Capture with Chemical Absorption: A state-of-the-art review." *Chemical Engineering Research and Design* 89 (9):1609-1624.

Wu, Xiaomei, Yunsong Yu, Zhen Qin, and Zaoxiao Zhang. 2014. "The Advances of Post-Combustion CO2 Capture with Chemical Solvents: Review and Guidelines." *Energy Procedia* 63:1339-1346.

Appendix 1 Technologies for CO_2 capture

As referred on Section 2.2, the main technologies available for CO_2 separation and capture are absorption, adsorption, cryogenics and membranes.

Adsorption is a physical process that involves the attachment of a gas or liquid to a solid surface and can occur on adsorber beds. This process requires flue gas streams with high CO_2 content because of the generally low capacity of most adsorbents. After the capture step, the adsorbent can be regenerated through the application of heat (temperature swing adsorption) or by the reduction of pressure (pressure swing adsorption). The most common adsorbents are activated carbon, alumina, metallic oxides and zeolites (Wang et al. 2011).

The absorption process can be either physical or chemical. The first one refers to the physical absorption of CO_2 into a solvent based on Henry's law. The flue gas stream fed to the absorber must have CO_2 partial pressures higher than 15 vol. % in order for the process to be economically feasible. The regeneration step can be achieved using heat, pressure reduction or the combination of both. Typical processes that use physical absorption are Selexol and Rectisol (Wang et al. 2011).

A representative scheme of the physical processes above mentioned is shown in Figure A1.1.

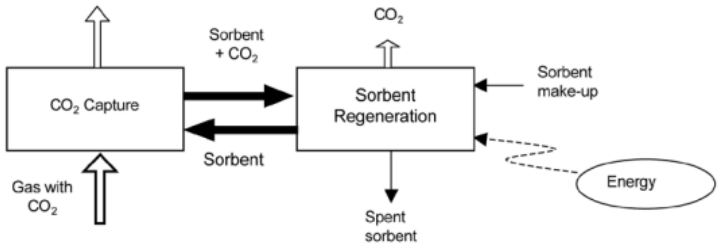

Figure A1. 1 - General scheme for separation with sorbents/solvents (Wang et al. 2011).

Cryogenic process achieves CO_2 separation from the flue gas by condensation as depicted in Figure A1.2, knowing that at atmospheric pressure, CO_2 condensates at -56.6 ^oC. This physical process is suitable for treating flue gas streams with high CO_2 concentrations considering the costs of refrigeration. This is typically used for CO_2 capture for oxy-fuel process (Wang et al. 2011).

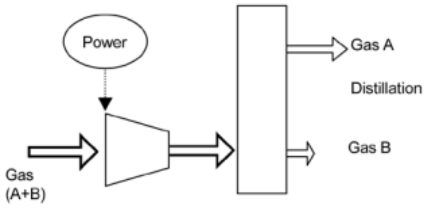

Figure A1. 2 - General scheme for cryogenics separation(Wang et al. 2011).

As illustrated in Figure A1.3, membranes processes are based on special materials that allow the selective permeation of gases through them. Their selectivity is related to the nature of the material, which usually consist of thin polymeric, metallic or ceramic films and separate mixtures based on the relative rates at which constituent species permeate. The driving force for the permeation is the difference in partial pressure of the components at either side of the membrane. Therefore, high pressure streams are usually preferred for membrane separation (Institute).

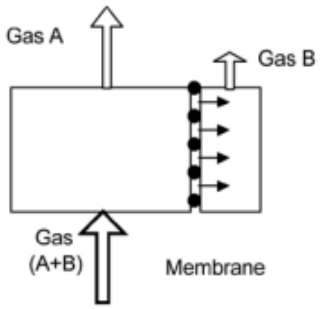

Figure A1. 3 - General scheme for membrane separation (Wang et al. 2011).

Besides post-combustion capture, which was described on Section 2, there are two other approaches for CCS: pre-combustion capture and oxy-combustion capture.

A1.1. Pre-combustion capture

Pre-combustion capture technology is mostly related to power plants based on the gasification of a fossil fuel, particularly IGCC.

Pre-combustion technology involves reacting the primary fuel with steam and/or air or oxygen. The gasification process is achieved through partial oxidation in the referred conditions and produces a mixture mainly composed of carbon monoxide and hydrogen, known as synthesis gas (syngas). Additional hydrogen, together with CO_2, is produced by reacting the carbon monoxide with steam in a water gas shift reactor. The resulting mixture is typically at a total pressure in the range of 20-70 bar and has a total CO_2 content between 15 and 60 vol. % on a dry basis. Carbon dioxide is removed from the syngas stream prior to the combustion of the hydrogen rich gas in the turbine for electricity generation purposes, as shown in Figure A1.4.

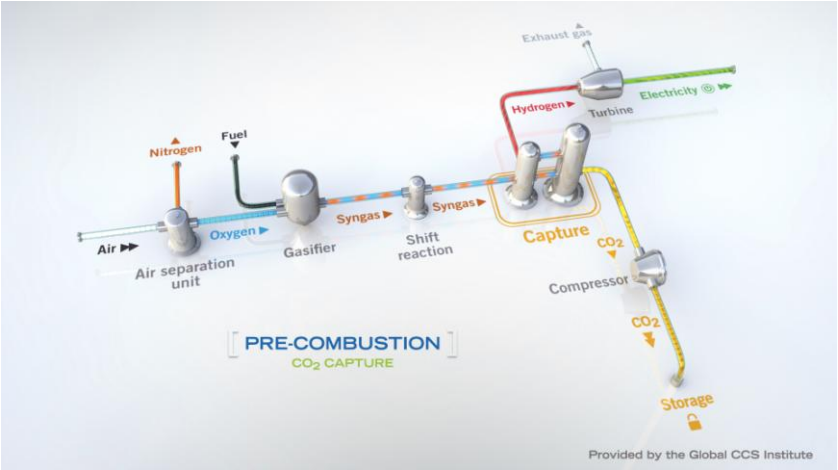

Figure A1. 4 – Schematic representation of a power plant with pre-combustion CO_2 capture (Institute).

The CO_2 removal technology used in pre-combustion capture is similar to the one used for natural gas purification and reforming, being based on the acid gas (i.e. CO_2, H_2S, COS) removal (AGR) process of absorption in a solvent followed by regenerative stripping of the rich solvent to release the CO_2 (Institute 2012).

Unlike PCC these processes are conducted at elevated pressure and/or high CO_2 content, allowing the absorption to be carried out not only with chemical solvents, but also with physical solvents (Institute 2012). Physical absorbents present a major advantage over chemical solvents since they can be regenerated through pressure reduction instead of thermal stripping, which significantly reduces the steam-heat requirements for solvent regeneration.

The inclusion of a pre-combustion capture unit in a IGCC plant leads to an increase in the energy penalty of around 21 % for a 90 % CO_2 absorption rate (Rubin et al. 2012).

A1.2. Oxy-fuel combustion capture

As can be seen in Figure A1.5, in oxy-fuel combustion plants the nitrogen is removed from the air in an Air Separation Unit (ASU) before the combustion, meaning that the primary fuel is burned under the presence of nearly pure oxygen (O_2 purity of 95-99 %). The absence of nitrogen leads to the production of a flue gas that is mainly water vapour and CO_2 – 70 to 90 % (dry basis) – of which around 80 % must be recycled to the boiler for temperature control (Institute January 2012a).

Depending on the local regulations, the non-recycled flue gas can be readily stored or may have to be purified first. If regulations allow, the raw gas can be dehydrated and directly compressed and stored, without any emissions. Otherwise, the flue gas impurities such as N_2, O_2 and Ar may have to be removed from the flue gas. In that case, the flue gas is partially

condensed at moderate pressure and a temperature of about -50 °C, at which the CO_2 condenses and the impurities do not. The liquefied CO_2 may further be purified in a distillation process, before being flashed and sent to storage. The non-condensed gases still have a CO_2 content of up to 35%, which can be removed through absorption or a membrane process, before being vented (Institute January 2012a).

As a method of CO_2 capture, oxy-fuel combustion systems are in the demonstration phase (Adegbulugbe et al. 2005).

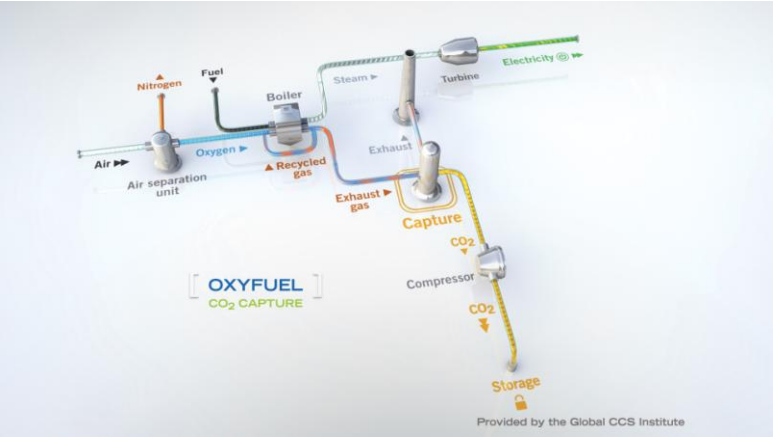

Figure A1. 5 - Schematic representation of a power plant with oxy-fuel combustion CO_2 capture (Institute).

Appendix 2 gCCS® library models

A2.1. Chemical Absorber (A)

Figure A2. 1 - Chemical absorber/stripper icon used in the gCCS® capture library.

One dimensional column based on the gPROMS® Advanced Model Library for Gas-Liquid Contactors (AML:GLC). This rate-based model is based on the two-film theory, according to which the liquid and gas bulk phases transfer heat and mass across the liquid and gas films, separated by an infinitesimally thin interface. It is considered chemical equilibrium in both bulk and films phases, as well as at the interface, where it is also assumed phase equilibrium. The heat and mass transfer in the two films are modelled according to Fick's law and the gSAFT thermodynamic model (see section 3.3) is used for the prediction of physical properties in each phase.

For the pressure drop correlation the model can apply the dry bed factor or Billet & Schultes correlations. For the calculation of mass transfer coefficients, this model considers Onda or Billet & Schultes correlations.

The absorber model requires the indication of the columns height and diameter, and the type of packing used.

A2.2. Chemical Stripper (ST)

Chemical stripper model is similar to the chemical absorber model except by the change in the thermodynamic model for physical properties prediction. gSAFT is also used, but modified in order to be more suited for the typical stripping operating conditions.

A2.3. Condenser (C)

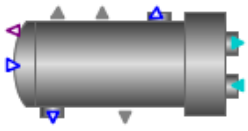

Figure A2. 2 - Condenser icon used in the gCCS® capture library.

This model is used for the simulation of a dynamic partial condenser, considering the use of a utility. It is assumed equilibrium between liquid and vapour phases, perfect mixture and that the cooling utility inlet and outlet is exclusively liquid.

The model requires the specification of the utility stream pressure drop and temperature increment and, if working in calibration mode, the operating temperature. Although vessel volume and diameter have to be specified, they are not relevant if operating in a steady state flowsheet.

A2.4. Flash drum (F)

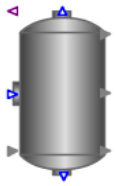

Figure A2. 3 - Flash drum icon used in the gCCS® capture library.

This vapour-liquid separator specification's requirements depend on the heat input chosen: manual, controlled or temperature specified. Regardless of the mode chosen, the initial phase (liquid, vapour or two-phase), volume and diameter must be specified.

When working in manual mode, the rate of energy input and the temperature initial guess must be defined as well. If the dynamic model is activated, pressure and initial conditions specifications are also required. For initial conditions specifications it can be set to be steady state and no values are required or the user can specify the pressure, mass fractions and either temperature or liquid level. If the controlled mode is chosen the rate of energy input doesn't have to be specified and the required variables are the same as for manual mode. When working in temperature specified mode, flash temperature must be specified instead of the temperature initial guess. This mode cannot be used with dynamics.

A2.5. Heat Exchanger (HX)

Figure A2. 4 - Heat Exchanger icon used in the gCCS® capture library.

This is a steady state model that simulates the heat exchange between two process streams, which may present a co-current or counter-current configuration. It is assumed a fixed heat transfer coefficient and pressure drop, which must be specified. No heat losses to the exterior or fouling are assumed.

In calibration mode, the outlet temperature of either the cold or the hot stream must be specified, or alternatively the temperature approach in one of the heat exchanger sides. For operational mode, the heat exchange area has to be specified.

A2.6. Heat Exchanger Process/Utility (HXU)

This model is similar to the heat exchanger presented previously, being one of the contact streams a utility. It requires the specification of the heat exchange applied to the process stream, if it is being cooled or heated.

In operational mode, besides the outlet temperature for the process stream, the temperature difference for the utility stream must also be specified, if its flow rate is set as calculated.

A2.7. Junction (M)

Figure A2. 5 - Junction icon used in the gCCS® capture library.

Steady state model applied to the mixing and/or splitting of a variable number of streams. In this model it is assumed no heat losses or pressure drop, ideal mixing and equal temperature, pressure and composition for the outlet streams.

The outlet pressures must be equalised or set to be equal to the minimum inlet pressure. The outlet flow rates may be set to be calculated by the downstream units, or calculated by specifying all but one split fraction/percentage. The system phase also has to be specified for initialisation purposes.

A2.8. Process sink (S)

Figure A2. 6 - Process sink icon used in the gCCS® capture library.

Model applied for the definition of a process stream leaving the flowsheet. It may be used for the calculation of a cumulative flow rate, in dynamic operation. Both the pressure and the flow rate may be calculated by upstream units or specified.

A2.9. Process source (SR)

Figure A2. 7 - Process source icon used in the gCCS® capture library.

This model provides the introduction of a material flow into the flowsheet. It is assumed to have infinite capacity, being able to calculate the cumulative solvent consumption in dynamic operation. The property estimation method is defined by the solvent choice.

As inputs, this model requires the specification of the temperature, composition and phase. The flowrate and the pressure can be chosen as specified or calculated by a downstream unit.

A2.10. Pump simple (P)

Figure A2. 8 - Pump simple icon used in the gCCS® capture library.

Isothermal and isenthalpic steady state model, used for the specification of a stream flow rate (manual mode) or its inlet/outlet pressures (advanced mode). The flow rate specification can be either done manually (through a value input) or set through the models control signal port, using a controller model. Due to the model simplicity, it can be used for the simulation of the pressure increase or decrease of both liquid and gas streams.

A2.11. Reboiler (R)

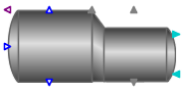

Figure A2. 9 - Reboiler icon used in the gCCS® capture library.

Dynamic model with energy and mass holdup for simulation of a boiling PZ solution. In this model it is assumed equilibrium between liquid and vapour phase, perfect mixing and the total condensation of the stream used as utility.

This model requires the specification of the stream pressure drop, initial phase, volume and diameter. In calibration mode the operating temperature must also be specified. For operational mode it is only required a temperature initial guess.

If the dynamic model is activated, the reboiler pressure must be specified, as well as the initial conditions. If heat losses are activated, the overall heat transfer coefficients must be specified for both liquid and vapour phases, as well as the ambient temperature.

A2.12. Recycle breaker (RB)

Figure A2. 10 - Recycle breaker icon used in the gCCS® capture library.

This is a model without physical meaning, which helps the initialisation of a recycle loop. Considering the initial state open, the inlet or outlet pressure and/or flow rate must be specified, as well as the temperature, composition and phase. The final state can be specified as open, acting as a source/sink; closed, and thus connecting the inlet and outlet streams; or make-up, being able to replace the solvent make-up model.

A2.13. Solvent make-up

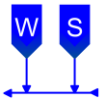

Figure A2. 11 - Solvent make-up icon used in the gCCS® capture library.

This model can be used instead of the recycle-breaker for solvent make-up purposes. It is able to calculate the amount of a specified solvent required to fulfil the respective mass fraction and total flowrate. The model requires the specification of the component not-closed and the solvents with make-up. In the present thesis, these are H_2O and PZ, respectively.

A2.14. Utility sink (SU)

Figure A2. 12 - Utility sink icon used in the gCCS® capture library.

Similar to the process sink, this model is used to define a utility stream leaving the flowsheet.

A2.15. Utility source (SRU)

Figure A2. 13 - Utility source icon used in the gCCS® capture library.

Model applied to the introduction of a water-based utility flow in the flowsheet. As in the source capture model, the temperature and phase must be specified, while the flowrate and pressure can be indicated or calculated by a downstream unit.

Appendix 3 Inputs for model validation

The data provided by Plaza and Rochelle, 2011, that was used for model validation was presented in Section 4.1, Table 4.1. The results provided regarding the pilot plant campaign conducted in November 2008 at the University of Texas at Austin had to be processed before being used for model validation.

The actual volumetric gas flow that was used throughout all fifteen runs was kept constant and equal to around $0.165\ \ \mathrm{m^3/s}$ ($P = 1\ \mathrm{atm}$ and $T = 40\ \ ^{\mathrm{o}}\mathrm{C}$).

The composition of the flue gas was also presented in Section 4.1. However, molar fractions were converted to mass fractions in order to facilitate consequent calculations.

First of all, using a one mole basis, the mass of each component was calculated. For H_2O:

$$Mass_{H_2O} = 18\ \mathrm{g/mol} \times 0.073\ \mathrm{mol/mol} \times 1\ \mathrm{mol} = 1.314\ \mathrm{g}$$

Same calculation was repeated for each component and the results were summed, resulting in a total value of 29.39 g. To obtain the mass fractions, each component's mass was divided by the sum of all values. Results are presented in Table A3.1.

Table A3. 1 - Flue gas molar and mass composition.

Component	Molar mass (g/mol)	Mole fraction	Mass (g)	Mass fraction
H_2O	18	0.073	1.31	0.045
CO_2	44	0.120	5.28	0.180
N_2	28	0.757	21.20	0.721
O_2	32	0.050	1.60	0.054

The gas molar flowrate, F_M, is calculated through equation A3.1.

$$F_M = \frac{P \times F_V}{R \times T} \qquad (A3.1)$$

Where P is the pressure (Pa), F_V is the volumetric flow ($m^3 \cdot s^{-1}$), R is the ideal gas constant ($\mathrm{m^3 \cdot Pa \cdot K^{-1} \cdot mol^{-1}}$) and T is the temperature (K).

The gas molar flowrate throughout the runs is 6.425 mol/s.

$$F_M = \frac{1.013 \times 10^5 \times 0.165}{8.314 \times (40 + 273.15)} = 6.425\ \mathrm{mol/s}$$

The liquid molar flowrate presented in Table A3.2 was obtained using this value and the L/G ratio provided on the paper.

The unit used for PZ concentration, molal, represents the molar amount of piperazine per mass of water. Thus, the molar fraction ratio between piperazine and water is given by equation A3.2.

$$\frac{x_{PZ}}{x_{H_2O}} = \frac{PZ\ concentration\ (\mathrm{m})}{H_2O\ molar\ mass\ (\mathrm{kg/mol})} \qquad (A3.2)$$

Using as a basis one mole of PZ, CO_2 molar quantity can be calculated using the lean loading and H_2O molar quantity using the ratio previously presented. As way of example, for Run 1:

$$\frac{x_{PZ}}{x_{H_2O}} = \frac{7.46\ \mathrm{mol_{PZ}/kg_{H_2O}}}{18 \times 10^{-3}\ \mathrm{kg_{H_2O}/mol_{H_2O}}} = 0.134\ \mathrm{mol_{PZ}/mol_{H_2O}}$$

$$CO_2\ molar\ quantity = 2\ \mathrm{mol\ PZ} \times Lean\ ldg\ (\mathrm{mol\ CO_2/2\ mol\ PZ}) = 2 \times 0.285 = 0.570\ \mathrm{mol}$$

$$H_2O\ molar\ quantity = \frac{1\ \mathrm{mol\ PZ}}{\frac{x_{PZ}}{x_{H_2O}}\ \mathrm{mol_{PZ}/mol_{H_2O}}} = \frac{1}{0.134} = 7.44\ \mathrm{mol}$$

Mole fractions are obtained by dividing the molar quantity of each component by the sum of all three, which corresponds in this case to 9.013 mol. Mass fractions are calculated as described before, for the flue gas composition. Its values are presented in Table A3.2.

Table A3. 2 - Inputs for model validation of the simple absorber.

Run	PZ conc. (m)	L/G (mol L/ mol G)	L (mol/s)	L (kg/s)	Lean loading (mol_{CO2}/ mol_{alk})	Mass fraction		
						PZ	CO_2	H_2O
1	7.46	5.5	35.34	0.9613	0.285	0.351	0.102	0.546
2	7.88	5.5	35.34	0.9793	0.308	0.351	0.111	0.517
3	9.18	4.9	31.48	0.9055	0.254	0.359	0.093	0.454
4	7.82	4.3	27.63	0.7615	0.284	0.275	0.080	0.407
5	8.22	6.0	38.55	1.0805	0.302	0.368	0.113	0.519
6	8.06	5.6	35.98	1.0032	0.305	0.363	0.113	0.523
7	7.85	6.7	43.04	1.1850	0.267	0.431	0.118	0.637
8	7.67	5.7	36.62	1.0103	0.331	0.354	0.120	0.536
9	7.60	6.8	45.61	1.1138	0.280	0.268	0.086	0.646
10	4.81	7.1	43.69	1.0683	0.316	0.276	0.077	0.647
11	4.95	6.8	35.34	0.8594	0.274	0.275	0.072	0.653
12	4.88	5.5	30.84	0.7420	0.257	0.265	0.071	0.664
13	4.64	4.8	43.69	1.1939	0.262	0.356	0.102	0.543
14	9	4.9	31.48	0.9017	0.266	0.390	0.106	0.503
15	8	5.4	34.69	0.9609	0.272	0.367	0.102	0.532

Using the total molar flowrate and the mole fractions calculated, the molar flowrate for each component was calculated. This molar flowrate was converted to mass flowrate for each component using the respective molar mass. The total mas flowrate presented in Table A3.2 is the sum of the flowrate for each component.

As mentioned in Section 4.2, intercooling was retrofitted to the existing absorber and two new experiments were conducted, being the available conditions and results presented in Table 4.5. Calculations made to obtain the input values presented in Table A3.3 were the same as for the simple absorber model.

Table A3. 3 - Inputs for model validation of the intercooled absorber.

Run	PZ conc. (m)	L/G (mol L/ mol G)	L (mol/s)	L (kg/s)	Lean loading (mol_{CO2}/ mol_{alk})	Mass fraction		
						PZ	CO_2	H_2O
1	7.5	4.5	28.91	0.7882	0.290	0.352	0.104	0.544
2	8.0	5.9	37.91	1.0531	0.297	0.364	0.109	0.527

Appendix 4 Heat duty calculation

Heat duty for each reboiler and heat exchanger was calculated as the energy provided by its utility stream through equation A4.1.

$$H(\mathrm{kJ/s}) = F \cdot C_P \cdot \Delta T + F \cdot \lambda \qquad (A4.1)$$

Where F is the utility mass flowrate (kg/s), C_P is the specific heat of saturated steam at specific conditions of temperature and pressure (kJ/(kg.K)), ΔT is the difference between inlet and outlet utility temperatures (K) and λ is the latent heat of vaporization (kJ/kg).

The utility used as hot stream throughout the processes and equipment analysed is saturated steam at 151 ºC and 5 bar. Utility physical properties contained in equation A4.1 are presented in Table A4.1.

Table A4. 1 - Physical properties of saturated steam at 151.85 ºC and 5 bar (Box).

λ (kJ/kg)	2107.42
C_P at 150 ºC and 5 bar (kJ/(kg.K))	2.3289

In order to ease process comparison, heat duty was also calculated relatively to the amount of CO_2 being stripped, dividing the energy requirement per time by the CO_2 stripped flowrate.

Results and deviations relatively to the first case are presented in Table A4.2.

Table A4. 2 - Heat duty results.

Case	$F_{utility}$ (kg/s)	ΔT	$F_{CO2\ stripped}$ (kg/s)	H_T (kJ/h)	Dev. (%)	H_T (kJ/kg CO_2)	Dev. (%)
A	0.0680	3.8	0.0295	9245	-	5229	-
B	0.0717	3.8	0.0330	9748	+5	4924	-6
C	0.0607	3.8	0.0304	8252	-11	4517	-14
D	0.0638	3.8	0.0330	8674	-6	4382	-16
E	0.0407	10.0	0.0212	5568	-40	2480	-16

Appendix 5 Inputs and results for process comparison

Table A5. 1 - Results for each source and sink model present on configuration A.

Unit		S_001	S_002	SR_001	SRU_001	SRU_002	SRU_003	SU_001	SU_002	SU_003
T (K)		324.6	310.0	313.2	298.2	298.2	424.0	308.1	308.1	420.2
P (bar)		1.00	1.38	1.01	1.01	1.01	4.50	0.91	0.91	4.40
F_i (kg/h)	H_2O	0.85	0.03	0.51	0.00	0.00	0.00	0.00	0.00	0.00
	PZ	0.04	0.00	0.00	0.00	0.00	0.00	0.00	0.00	0.00
	CO_2	0.02	1.77	2.04	0.00	0.00	0.00	0.00	0.00	0.00
	N_2	8.15	0.00	8.18	0.00	0.00	0.00	0.00	0.00	0.00
	O_2	0.61	0.00	0.62	0.00	0.00	0.00	0.00	0.00	0.00
	Cooling water	0.00	0.00	0.00	123.00	60.00	0.00	123.00	60.00	0.00
	Steam	0.00	0.00	0.00	0.00	0.00	4.04	0.00	0.00	4.04
F_T (kg/h)		9.90	1.81	11.34	123.00	60.00	4.04	123.00	60.00	4.04
Mass fraction	H_2O	0.086	0.018	0.045	0.000	0.000	0.000	0.000	0.000	0.000
	PZ	0.004	0.001	0.000	0.000	0.000	0.000	0.000	0.000	0.000
	CO_2	0.002	0.979	0.180	0.000	0.000	0.000	0.000	0.000	0.000
	N_2	0.823	0.001	0.721	0.000	0.000	0.000	0.000	0.000	0.000
	O_2	0.062	0.000	0.054	0.000	0.000	0.000	0.000	0.000	0.000
	Cooling water	0.000	0.000	0.000	1.000	1.000	0.000	1.000	1.000	0.000
	Steam	0.000	0.000	0.000	0.000	0.000	1.000	0.000	0.000	1.000
% Liquid		0	0	0	1	1	0	1	1	1

Table A5. 2 - Results for each source and sink model present on configuration B.

Unit		S_001	S_002	SR_001	SRU_001	SRU_002	SRU_003	SRU_004	SU_001	SU_002	SU_003	SU_004
T (K)		313.2	310.0	313.2	298.2	298.2	298.1	242.0	308.1	308.1	308.1	420.2
P (bar)		1.00	1.38	1.01	1.01	1.01	1.01	4.50	0.91	0.91	0.91	4.40
F_i (kg/h)	H_2O	0.39	0.04	0.51	0.00	0.00	0.00	0.00	0.00	0.00	0.00	0.00
	PZ	0.01	0.00	0.00	0.00	0.00	0.00	0.00	0.00	0.00	0.00	0.00
	CO_2	0.03	1.98	2.04	0.00	0.00	0.00	0.00	0.00	0.00	0.00	0.00
	N_2	8.20	0.00	8.18	0.00	0.00	0.00	0.00	0.00	0.00	0.00	0.00
	O_2	0.62	0.00	0.62	0.00	0.00	0.00	0.00	0.00	0.00	0.00	0.00
	Cooling water	0.00	0.00	0.00	55.62	102.00	62.40	0.00	55.62	102.00	62.40	0.00
	Steam	0.00	0.00	0.00	0.00	0.00	0.00	4.30	0.00	0.00	0.00	4.30
F_T (kg/h)		9.24	2.02	11.34	55.62	102.00	62.40	4.30	55.62	102.00	62.40	4.30
Mass fraction	H_2O	0.042	0.018	0.045	0.000	0.000	0.000	0.000	0.000	0.000	0.000	0.000
	PZ	0.001	0.001	0.000	0.000	0.000	0.000	0.000	0.000	0.000	0.000	0.000
	CO_2	0.003	0.979	0.180	0.000	0.000	0.000	0.000	0.000	0.000	0.000	0.000
	N_2	0.887	0.001	0.721	0.000	0.000	0.000	0.000	0.000	0.000	0.000	0.000
	O_2	0.067	0.000	0.054	0.000	0.000	0.000	0.000	0.000	0.000	0.000	0.000
	Cooling water	0.000	0.000	0.000	1.000	1.000	1.000	0.000	1.000	1.000	1.000	0.000
	Steam	0.000	0.000	0.000	0.000	0.000	0.000	1.000	0.000	0.000	0.000	1.000
% Liquid		0	0	0	1	1	1	0	1	1	1	1

Table A5. 3 - Results for each source and sink model present on configuration C.

Unit		S_001	S_002	SR_001	SRU_001	SRU_002	SRU_003	SU_001	SU_002	SU_003
T (K)		324.7	310.0	313.2	298.2	298.2	424.0	308.1	308.1	420.2
P (bar)		1.00	1.38	1.01	1.01	1.01	4.50	0.91	0.91	4.40
F_i (kg/h)	H_2O	0.86	0.03	0.51	0.00	0.00	0.00	0.00	0.00	0.00
	PZ	0.04	0.00	0.00	0.00	0.00	0.00	0.00	0.00	0.00
	CO_2	0.19	1.83	2.04	0.00	0.00	0.00	0.00	0.00	0.00
	N_2	8.15	0.00	8.18	0.00	0.00	0.00	0.00	0.00	0.00
	O_2	0.61	0.00	0.62	0.00	0.00	0.00	0.00	0.00	0.00
	Cooling water	0.00	0.00	0.00	100.80	64.20	0.00	100.80	64.20	0.00
	Steam	0.00	0.00	0.00	0.00	0.00	3.64	0.00	0.00	3.64
F_T (kg/h)		9.84	1.87	11.34	100.80	64.20	3.64	100.80	64.20	3.64
Mass fraction	H_2O	0.088	0.019	0.045	0.000	0.000	0.000	0.000	0.000	0.000
	PZ	0.004	0.001	0.000	0.000	0.000	0.000	0.000	0.000	0.000
	CO_2	0.019	0.979	0.180	0.000	0.000	0.000	0.000	0.000	0.000
	N_2	0.828	0.001	0.721	0.000	0.000	0.000	0.000	0.000	0.000
	O_2	0.062	0.000	0.054	0.000	0.000	0.000	0.000	0.000	0.000
	Cooling water	0.000	0.000	0.000	1.000	1.000	0.000	1.000	1.000	0.000
	Steam	0.000	0.000	0.000	0.000	0.000	1.000	0.000	0.000	1.000
% Liquid		0	0	0	1	1	0	1	1	1

Table A5. 4 - Results for each source and sink model present on configuration D.

Unit		S_001	S_002	SR_001	SRU_001	SRU_002	SRU_003	SRU_004	SU_001	SU_002	SU_003	SU_004
T (K)		313.1	310.0	313.2	298.2	298.2	298.2	424.0	303.1	308.1	308.1	420.2
P (bar)		1.00	1.38	1.01	1.01	1.01	1.01	4.50	0.91	0.91	0.91	4.40
F_i (kg/h)	H_2O	0.39	0.04	0.51	0.00	0.00	0.00	0.00	0.00	0.00	0.00	0.00
	PZ	0.01	0.00	0.00	0.00	0.00	0.00	0.00	0.00	0.00	0.00	0.00
	CO_2	0.02	1.99	2.04	0.00	0.00	0.00	0.00	0.00	0.00	0.00	0.00
	N_2	8.14	0.00	8.18	0.00	0.00	0.00	0.00	0.00	0.00	0.00	0.00
	O_2	0.61	0.00	0.62	0.00	0.00	0.00	0.00	0.00	0.00	0.00	0.00
	Cooling water	0.00	0.00	0.00	50.10	82.80	66.00	0.00	50.10	82.80	66.00	0.00
	Steam	0.00	0.00	0.00	0.00	0.00	0.00	3.83	0.00	0.00	0.00	3.83
F_T (kg/h)		9.18	2.03	11.34	50.10	82.80	66.00	3.83	50.10	82.80	66.00	3.83
Mass fraction	H_2O	0.042	0.018	0.045	0.000	0.000	0.000	0.000	0.000	0.000	0.000	0.000
	PZ	0.001	0.001	0.000	0.000	0.000	0.000	0.000	0.000	0.000	0.000	0.000
	CO_2	0.003	0.979	0.180	0.000	0.000	0.000	0.000	0.000	0.000	0.000	0.000
	N_2	0.887	0.001	0.721	0.000	0.000	0.000	0.000	0.000	0.000	0.000	0.000
	O_2	0.067	0.000	0.054	0.000	0.000	0.000	0.000	0.000	0.000	0.000	0.000
	Cooling water	0.000	0.000	0.000	1.000	1.000	1.000	0.000	1.000	1.000	1.000	0.000
	Steam	0.000	0.000	0.000	0.000	0.000	0.000	1.000	0.000	0.000	0.000	1.000
% Liquid		0	0	0	1	1	1	0	1	1	1	1

Table A5. 5 - Results for each source and sink model present on configuration E.

Unit		S_001	S_002	SR_001	SRU_001	SRU_002	SRU_003	SU_001	SU_002	SU_003
T (K)		335.0	310.0	313.2	293.2	424.0	298.1	303.1	414.0	308.1
P (bar)		1.00	5.40	1.01	1.01	4.50	1.00	0.91	4.40	0.90
F_i (kg/h)	H_2O	1.41	0.01	0.51	0.00	0.00	0.00	0.00	0.00	0.00
	PZ	0.09	0.00	0.00	0.00	0.00	0.00	0.00	0.00	0.00
	CO_2	0.75	1.27	2.04	0.00	0.00	0.00	0.00	0.00	0.00
	N_2	8.17	0.00	8.18	0.00	0.00	0.00	0.00	0.00	0.00
	O_2	0.62	0.00	0.62	0.00	0.00	0.00	0.00	0.00	0.00
	Cooling water	0.00	0.00	0.00	69.60	0.00	45.36	69.60	2.44	45.36
	Steam	0.00	0.00	0.00	0.00	2.44	0.00	0.00	0.00	0.00
F_T (kg/h)		11.04	1.28	11.34	69.60	2.44	45.36	69.60	2.44	45.36
Mass fraction	H_2O	0.128	0.005	0.045	0.000	0.000	0.000	0.000	0.000	0.000
	PZ	0.008	0.001	0.000	0.000	0.000	0.000	0.000	0.000	0.000
	CO_2	0.068	0.992	0.180	0.000	0.000	0.000	0.000	0.000	0.000
	N_2	0.740	0.002	0.721	0.000	0.000	0.000	0.000	0.000	0.000
	O_2	0.056	0.000	0.054	0.000	0.000	0.000	0.000	0.000	0.000
	Cooling water	0.000	0.000	0.000	1.000	0.000	1.000	1.000	1.000	1.000
	Steam	0.000	0.000	0.000	0.000	1.000	0.000	0.000	0.000	0.000
% Liquid		0	0	0	1	0	0	1	1	1

Table A5. 6 - Design parameters and operating conditions for Case A.

Unit		Parameter	Value
Absorber		Diameter (m)	0.427
		Height (m)	6.10
Stripper		Diameter (m)	0.427
		Height (m)	6.10
Heat exchanger		Cold stream outlet temperature (K)	370
Lean solvent cooler		Process stream outlet temperature (K)	313.15
Reboiler		Temperature (K)	380
		Pressure (Pa)	1.38×10^5
Condenser		Temperature (K)	310
Lean solvent		F (kg/s)	1.000
		PZ mass fraction	0.364
Pump	P_001	Inlet pressure (Pa)	9.13×10^4
		Outlet pressure (Pa)	1.38×10^5
		F (kg/h)	1.02
	P_002	Inlet pressure (Pa)	1.01×10^5
		Outlet pressure (Pa)	1.01×10^5
		F (kg/h)	1.00
	P_003	Inlet pressure (Pa)	1.38×10^5
		Outlet pressure (Pa)	1.38×10^5
		F (kg/h)	1.05
	P_004	Inlet pressure (Pa)	1.38×10^5
		Outlet pressure (Pa)	1.21×10^5
		F (kg/h)	0.99
	P_005	Inlet pressure (Pa)	1.01×10^5
		Outlet pressure (Pa)	1.01×10^5
		F (kg/h)	1.02

Table A5. 7 - Design parameters and operating conditions for Case B.

Unit		Parameter	Value
Absorber		Diameter (m)	0.427
		Height (m)	6.10 (IC at the middle)
Stripper		Diameter (m)	0.427
		Height (m)	6.10
Heat exchanger		Cold stream outlet temperature (K)	370
Lean solvent cooler		Process stream outlet temperature (K)	313.15
Reboiler		Temperature (K)	380
		Pressure (Pa)	1.38×10^5
Condenser		Temperature (K)	310
Lean solvent		F (kg/s)	1.000
		PZ mass fraction	0.364
Pump	P_001	Inlet pressure (Pa)	1.38×10^5
		Outlet pressure (Pa)	1.38×10^5
		F (kg/h)	1.07
	P_002	Inlet pressure (Pa)	1.38×10^5
		Outlet pressure (Pa)	1.21×10^5
		F (kg/h)	1.00
	P_003	Inlet pressure (Pa)	1.01×10^5
		Outlet pressure (Pa)	1.01×10^5
		F (kg/h)	1.03
	P_004	Inlet pressure (Pa)	9.13×10^4
		Outlet pressure (Pa)	1.38×10^5
		F (kg/h)	1.03
	P_005	Inlet pressure (Pa)	1.01×10^5
		Outlet pressure (Pa)	1.01×10^5
		F (kg/h)	1.00
	P_006	Inlet pressure (Pa)	9.07×10^4
		Outlet pressure (Pa)	1.01×10^5
		F (kg/h)	1.02

Table A5. 8 – Design parameters and operating conditions for Case C.

Unit		Parameter	Value
Absorber		Diameter (m)	0.427
		Height (m)	6.10
Stripper		Diameter (m)	0.427
		Height (m)	6.10
Heat exchanger		Cold stream outlet temperature (K)	370
Lean solvent cooler		Process stream outlet temperature (K)	313.15
Reboiler		Temperature (K)	380
		Pressure (Pa)	1.38×10^5
Condenser		Temperature (K)	310
Lean solvent		F (kg/s)	1.000
		PZ mass fraction	0.364
Pump	P_001	Inlet pressure (Pa)	9.13×10^4
		Outlet pressure (Pa)	1.38×10^5
		F (kg/h)	1.02
	P_002	Inlet pressure (Pa)	9.13×10^4
		Outlet pressure (Pa)	1.00×10^5
		F (kg/h)	1.00
	P_003	Inlet pressure (Pa)	1.01×10^5
		Outlet pressure (Pa)	1.01×10^5
		F (kg/h)	1.02
	P_004	Inlet pressure (Pa)	1.38×10^5
		Outlet pressure (Pa)	1.38×10^5
		F (kg/h)	1.06
	P_005	Inlet pressure (Pa)	1.38×10^5
		Outlet pressure (Pa)	1.11×10^5
		F (kg/h)	1.00
	P_006	Inlet pressure (Pa)	1.11×10^5
		Outlet pressure (Pa)	1.38×10^5
		F (kg/h)	0.009
Flash		Temperature initial guess (K)	380

Table A5. 9 - Design parameters and operating conditions for Case D.

Unit		Parameter	Value
Absorber		Diameter (m)	0.427
		Height (m)	6.10
Stripper		Diameter (m)	0.427
		Height (m)	6.10 (IC at the middle)
Heat exchanger		Cold stream outlet temperature (K)	370
Lean solvent cooler		Process stream outlet temperature (K)	313.15
Reboiler		Temperature (K)	380
		Pressure (Pa)	1.38×10^5
Condenser		Temperature (K)	310
Lean solvent		F (kg/s)	1.000
		PZ mass fraction	0.364
Pump	P_001	Inlet pressure (Pa)	9.11×10^4
		Outlet pressure (Pa)	1.38×10^5
		F (kg/h)	1.03
	P_002	Inlet pressure (Pa)	1.11×10^5
		Outlet pressure (Pa)	1.38×10^5
		F (kg/h)	0.009
	P_003	Inlet pressure (Pa)	9.20×10^4
		Outlet pressure (Pa)	1.00×10^5
		F (kg/h)	1.00
	P_004	Inlet pressure (Pa)	9.06×10^4
		Outlet pressure (Pa)	1.01×10^5
		F (kg/h)	1.01
	P_005	Inlet pressure (Pa)	1.38×10^5
		Outlet pressure (Pa)	1.38×10^5
		F (kg/h)	1.07
	P_006	Inlet pressure (Pa)	1.38×10^5
		Outlet pressure (Pa)	1.11×10^5
		F (kg/h)	1.01
Flash		Temperature initial guess (K)	380

Table A5. 10 - Design parameters and operating conditions for Case E.

Unit		Parameter	Value
Absorber		Diameter (m)	0.427
		Height (m)	6.10
Stripper		Diameter (m)	0.427
		Height (m)	6.10
Heat exchanger		Cold stream outlet temperature (K)	370
Lean solvent cooler		Process stream outlet temperature (K)	313.15
HP Flash Heater		Process stream outlet temperature (K)	423
Condenser		Temperature (K)	310
Lean solvent		F (kg/s)	1.000
		PZ mass fraction	0.364
Pump	P_001	Inlet pressure (Pa)	1.13×10^5
		Outlet pressure (Pa)	1.00×10^5
		F (kg/h)	1.00
	P_002	Inlet pressure (Pa)	9.07×10^4
		Outlet pressure (Pa)	1.00×10^5
		F (kg/h)	1.00
	P_003	Inlet pressure (Pa)	9.11×10^4
		Outlet pressure (Pa)	1.00×10^6
		F (kg/h)	1.01
	P_004	Inlet pressure (Pa)	9.95×10^5
		Outlet pressure (Pa)	5.50×10^5
		F (kg/h)	1.00
	P_005	Inlet pressure (Pa)	5.32×10^5
		Outlet pressure (Pa)	1.13×10^5
		F (kg/h)	1.07
Flash		Temperature initial guess (K)	380

Appendix 6 Equilibrium line calculation

Since there is no publically available information regarding the equilibrium between CO_2 and aqueous piperazine at these specific conditions, the equilibrium line had to be determined.

For this purpose, the model presented in Figure A3.1 was assembled on gPROMS®. The flash drum is fed with lean solvent at the conditions used in the absorber columns for intercooling effect studies, and with a CO_2 stream, both presented in Table A6.1.

The outlet liquid stream is CO_2 saturated, therefore representing the equilibrium.

Table A6. 1 - Input conditions.

Stream	SR_001	SR_002
F (kg/s)	1	2
P (Pa)	1.01×10^3	1.01×10^3
T (K)	313.15	370.00
w_{H2O}	0.544	0.100
w_{PZ}	0.352	0.000
w_{CO2}	0.104	0.900

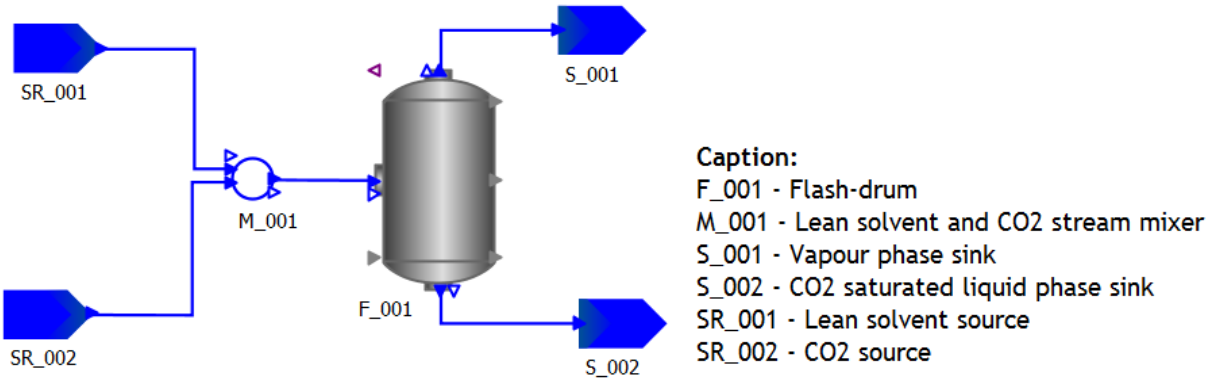

Figure A6. 1 - Model used for equilibrium line determination.

Flash model was operated in the "Temperature Specified" mode and its temperature was varied between 295 and 350 K to obtain the equilibrium line shown in Figure A6.2, whose equation is presented below (A6.1).

$$CO_2 loading\ (\text{mol } CO_2/\text{mol alk}) = -2.24 \times 10^{-5} T(\text{K}) + 0.0124515\ T(\text{K}) - 1.2359947 \qquad (A6.1)$$

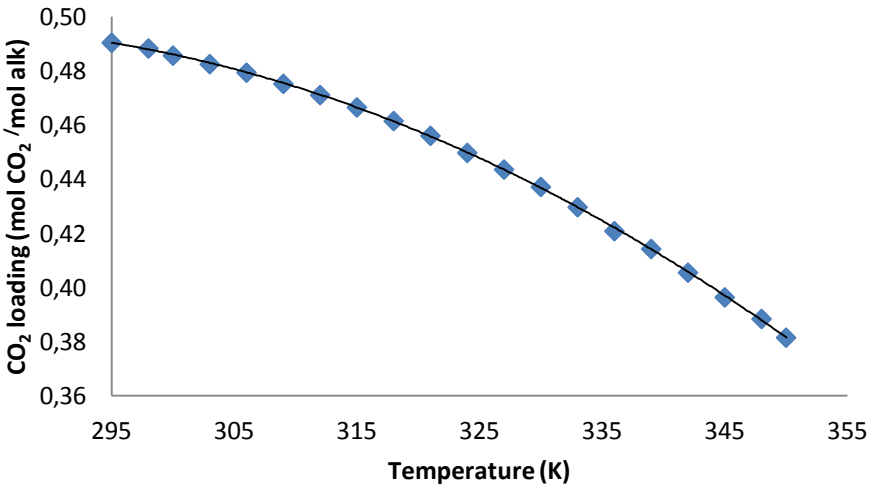

Figure A6. 2 - Equilibrium line between CO_2 and aqueous piperazine.

A comparison between operating and equilibrium values along the column is presented in Tables A6.2, A6.3 and A6.4 for an absorber with middle bottom intercooling, middle top intercooling and without intercooling, respectively.

Table A6. 2 - Operating, equilibrium and driving force values along an absorber with middle bottom intercooling.

Z/Z_T	T_{liq} (K)	CO_2 loading (mol $_{CO2}$ / mol $_{alk}$)		Driving force
		Operating	Equilibrium	
0.00	313.15	0.289	0.467	0.177
0.10	319.40	0.300	0.456	0.156
0.20	330.14	0.319	0.433	0.114
0.30	332.82	0.325	0.427	0.102
0.40	333.06	0.328	0.426	0.098
0.50	332.46	0.330	0.428	0.097
0.60	331.11	0.335	0.431	0.096
0.66	329.44	0.339	0.435	0.096
0.70	**313.15**	**0.347**	**0.467**	**0.120**
0.75	321.58	0.369	0.452	0.083
0.80	323.30	0.374	0.448	0.075
0.85	323.57	0.375	0.448	0.073
0.90	323.47	0.375	0.448	0.073
0.95	323.04	0.376	0.449	0.072
1.00	321.83	0.379	0.451	0.072

Table A6. 3 - Operating, equilibrium and driving force values along an absorber with middle top intercooling.

Z/Z_T	T_{liq} (K)	CO_2 loading (mol $_{CO2}$ / mol $_{alk}$)		Driving force
		Operating	Equilibrium	
0.00	313.15	0.289	0.467	0.177
0.05	325.94	0.312	0.443	0.131
0.10	331.11	0.322	0.431	0.109
0.15	332.40	0.327	0.428	0.101
0.20	332.17	0.330	0.428	0.099
0.25	331.09	0.334	0.431	0.097
0.30	328.98	0.339	0.436	0.097
0.34	**313.15**	**0.346**	**0.467**	**0.121**
0.37	318.12	0.359	0.458	0.099
0.40	320.84	0.366	0.453	0.087
0.45	322.29	0.370	0.450	0.080
0.50	323.44	0.373	0.448	0.075
0.60	323.79	0.374	0.447	0.073
0.70	323.75	0.374	0.447	0.073
0.80	323.49	0.375	0.448	0.073
0.90	322.68	0.377	0.450	0.072
1.00	319.94	0.383	0.455	0.072

Table A6. 4 - Operating, equilibrium and driving force values along an absorber without intercooling.

Z/Z_T	T_{liq} (K)	CO_2 loading (mol $_{CO2}$ / mol $_{alk}$)		Driving force
		Operating	Equilibrium	
0.00	313.15	0.289	0.467	0.177
0.05	324.38	0.311	0.446	0.135
0.10	330.44	0.323	0.433	0.109
0.15	333.26	0.329	0.426	0.097
0.20	334.48	0.332	0.423	0.091
0.25	334.96	0.333	0.422	0.088
0.30	335.12	0.334	0.421	0.087
0.35	335.12	0.335	0.421	0.086
0.40	335.04	0.335	0.421	0.086
0.45	334.91	0.336	0.422	0.086
0.50	334.73	0.336	0.422	0.086
0.55	334.51	0.337	0.423	0.085
0.60	334.24	0.338	0.423	0.085
0.65	333.89	0.339	0.424	0.085
0.70	333.45	0.341	0.425	0.085
0.75	332.90	0.343	0.427	0.084
0.80	332.17	0.345	0.428	0.084
0.85	331.20	0.348	0.431	0.083
0.90	329.88	0.352	0.434	0.082
0.95	327.96	0.357	0.438	0.081
1.00	325.02	0.365	0.445	0.080

Appendix 7 Stripper pressure and temperature effect

Table A7. 1 - Stripper pressure and temperature effect.

Stripper P (Pa)	Reboiler T (K)	F_{Steam} (kg/s)	F CO_2 stripped (kg/s)	Heat duty reboiler (kJ/s)	Heat duty (kJ/kg CO_2 stripped)	Deviation heat duty (%)	CO_2 capture (%)	Loading (mol $_{CO2}$/ mol $_{alk}$)	
								Lean	Rich
$1.38\times \mathbf{10^5}$	380.0	0.0674	2.95×10^{-2}	152.66	5749	-	88.2	0.266	0.347
$1.40\times \mathbf{10^5}$	380.4	0.0672	2.95×10^{-2}	152.32	5745	-0.06	88.1	0.267	0.347
$1.45\times \mathbf{10^5}$	381.3	0.0671	2.95×10^{-2}	152.07	5734	-0.25	88.1	0.267	0.347
$1.50\times \mathbf{10^5}$	382.2	0.0670	2.95×10^{-2}	151.85	5729	-0.34	88.1	0.267	0.347
$1.55\times \mathbf{10^5}$	383.1	0.0669	2.95×10^{-2}	151.64	5718	-0.52	88.1	0.267	0.347
$1.60\times \mathbf{10^5}$	384.0	0.0668	2.95×10^{-2}	151.44	5711	-0.65	88.1	0.267	0.347
$1.65\times \mathbf{10^5}$	384.8	0.0668	2.95×10^{-2}	151.26	5704	-0.77	88.1	0.267	0.347
$1.70\times \mathbf{10^5}$	385.6	0.0667	2.95×10^{-2}	151.09	5695	-0.94	88.1	0.267	0.347
$1.75\times \mathbf{10^5}$	386.4	0.0666	2.95×10^{-2}	150.93	5691	-1.00	88.1	0.267	0.347
$1.80\times \mathbf{10^5}$	387.2	0.0665	2.95×10^{-2}	150.78	5682	-1.15	88.1	0.267	0.347
$1.85\times \mathbf{10^5}$	388.0	0.0665	2.95×10^{-2}	150.64	5679	-1.21	88.1	0.267	0.347
$1.90\times \mathbf{10^5}$	388.7	0.0664	2.95×10^{-2}	150.51	5670	-1.36	88.1	0.267	0.347
$1.95\times \mathbf{10^5}$	389.4	0.0664	2.95×10^{-2}	150.38	5668	-1.41	88.1	0.267	0.347
$2.00\times \mathbf{10^5}$	390.1	0.0663	2.95×10^{-2}	150.26	5661	-1.51	88.1	0.267	0.347
$2.05\times \mathbf{10^5}$	390.8	0.0663	2.95×10^{-2}	150.14	5657	-1.60	88.1	0.267	0.347

Table A7. 2 - Stripper pressure and temperature effect (continued).

Stripper P (Pa)	Reboiler T (K)	F_{Steam} (kg/s)	F CO_2 stripped (kg/s)	Heat duty reboiler (kJ/s)	Heat duty (kJ/kg CO_2 stripped)	Deviation heat duty (%)	CO_2 capture (%)	Loading (mol $_{CO2}$/ mol $_{alk}$)	
								Lean	Rich
$2.10\times \mathbf{10^5}$	391.5	0.0662	2.95×10^{-2}	150.03	5654	-1.64	88.1	0.267	0.347
$2.15\times \mathbf{10^5}$	392.2	0.0662	2.95×10^{-2}	149.93	5646	-1.78	88.1	0.267	0.347
$2.20\times \mathbf{10^5}$	392.8	0.0661	2.95×10^{-2}	149.83	5644	-1.82	88.1	0.267	0.347
$2.25\times \mathbf{10^5}$	393.5	0.0661	2.95×10^{-2}	149.73	5642	-1.86	88.1	0.267	0.347
$2.30\times \mathbf{10^5}$	394.1	0.0660	2.95×10^{-2}	149.64	5634	-1.99	88.1	0.267	0.347
$2.35\times \mathbf{10^5}$	394.7	0.0660	2.95×10^{-2}	149.55	5632	-2.03	88.1	0.267	0.347
$2.40\times \mathbf{10^5}$	395.3	0.0660	2.95×10^{-2}	149.47	5630	-2.06	88.1	0.267	0.347
$2.45\times \mathbf{10^5}$	395.9	0.0659	2.95×10^{-2}	149.39	5623	-2.19	88.1	0.267	0.347
$2.50\times \mathbf{10^5}$	396.5	0.0659	2.95×10^{-2}	149.31	5621	-2.22	88.1	0.267	0.347

Appendix 8 L/G ratio effect

Table A8. 1 - L/G ratio effect on Case A.

L (mol/s)	L/G	Loading (mol $_{CO2}$/ mol $_{alk}$)		CO_2 capture (%)	Heat duty (kJ/s)	F_{CO2} stripped (kg/s)	Heat duty (kJ/kg CO_2)
		Lean	Rich				
25.000	3.9	0.266	0.346	89.0	141.579	0.030	4746
24.902	3.9	0.266	0.346	88.8	141.239	0.030	4744
24.779	3.9	0.266	0.346	88.6	140.813	0.030	4742
24.656	3.8	0.266	0.346	88.4	140.386	0.030	4739
24.534	3.8	0.266	0.347	88.2	139.958	0.030	4736
24.411	3.8	0.266	0.347	88.0	139.529	0.029	4733
24.166	3.8	0.266	0.347	87.6	138.667	0.029	4728
24.043	3.7	0.266	0.347	87.3	138.235	0.029	4725
23.920	3.7	0.266	0.348	87.1	137.802	0.029	4723
23.675	3.7	0.266	0.348	86.7	136.933	0.029	4717
23.552	3.7	0.266	0.348	86.5	136.497	0.029	4714
23.430	3.6	0.266	0.349	86.3	136.060	0.029	4711
23.307	3.6	0.266	0.349	86.1	135.622	0.029	4709
23.160	3.6	0.266	0.349	85.8	135.095	0.029	4705
23.013	3.6	0.266	0.349	85.5	134.568	0.029	4702
22.841	3.6	0.266	0.350	85.2	133.950	0.029	4698
22.669	3.5	0.266	0.350	84.9	133.331	0.028	4694
22.497	3.5	0.266	0.350	84.6	132.710	0.028	4690
22.350	3.5	0.266	0.351	84.3	132.177	0.028	4686
22.203	3.5	0.266	0.351	84.1	131.642	0.028	4683
22.031	3.4	0.266	0.351	83.8	131.016	0.028	4679
21.884	3.4	0.266	0.351	83.5	130.479	0.028	4675
21.712	3.4	0.266	0.352	83.2	129.850	0.028	4671
21.516	3.3	0.266	0.352	82.8	129.129	0.028	4666
21.320	3.3	0.266	0.353	82.5	128.406	0.028	4661
21.099	3.3	0.266	0.353	82.0	127.590	0.027	4656
20.878	3.2	0.266	0.354	81.6	126.770	0.027	4650
20.854	3.2	0.266	0.354	81.6	126.679	0.027	4650

Appendix 9 Piperazine concentration effect

Table A9. 1 - Piperazine concentration effect on Case A.

w_{PZ}	Rich loading (mol CO_2/ mol alk)	CO_2 capture (%)	F_{CO2} stripped (kg/s)	Heat duty (kJ/kg CO_2)
0.375	0.346	88.4	0.0296	4720
0.370	0.346	88.3	0.0296	4727
0.360	0.347	88.1	0.0295	4742
0.350	0.348	87.8	0.0294	4757
0.340	0.349	87.4	0.0292	4773
0.330	0.349	87.0	0.0291	4790
0.320	0.351	86.4	0.0289	4808
0.310	0.352	85.8	0.0287	4828
0.300	0.353	85.1	0.0284	4849
0.290	0.354	84.3	0.0281	4872
0.280	0.356	83.5	0.0278	4897
0.270	0.357	82.5	0.0275	4925
0.260	0.359	81.4	0.0271	4954
0.250	0.360	80.3	0.0267	4987
0.240	0.362	79.0	0.0263	5023
0.230	0.364	77.6	0.0258	5063
0.220	0.366	76.1	0.0253	5106
0.210	0.368	74.5	0.0248	5154
0.200	0.370	72.8	0.0242	5207
0.190	0.372	71.0	0.0236	5266
0.180	0.375	69.0	0.0229	5331
0.170	0.377	67.0	0.0222	5405
0.160	0.380	64.8	0.0215	5488
0.150	0.383	62.4	0.0207	5583